Delft University of Technology

MASTER OF SCIENCE THESIS

Monin-Obukhov Similarity Theory Applied to Offshore Wind Data

Validation of Models to Estimate the Offshore Wind Speed Profile in the North Sea

Andrea Venora

Delft, 5th August 2009

DELFT UNIVERSITY OF TECHNOLOGY

WIND ENERGY SECTION

The undersigned hereby certify that they have read and recommend to the Faculty of Aerospace Engineering for acceptance a thesis entitled “Monin-Obukhov Similarity Theory Applied to Offshore Wind Data” by Andrea Venora in fulfillment of the requirements for the degree of Master of Science.

Supervisor:

ir. A. Sathe

____

Readers:

prof. dr. G.J.W van Bussel

____

dr. ir. W. Bierbooms

____

dr. A. Brand

____

Delft, 5th August 2009

"Ecco io sono con voi tutti i giorni,

fino alla fine del Mondo."

Mt. 28,20

...alla mia famiglia

ACKNOWLEDGEMENTS

In the first place, I would like to express special thanks to my supervisor, Ameya Sathe, for his support and guidance, for having patiently helped and encouraged me, through this scientific work, any time it was necessary over the last year and half. Special recognition is also due all the staff of the Wind Energy Department of Aerospace Faculty at TU Delft; because from them, I have learned a lot about the wind energy world over these three years. I would like to acknowledge the support of Ing. Salvo Sciuto and Dott. Francesco Bonomo in the first steps of my work during the internship at ENEL *Produzione* S.p.A. in Catania. A special acknowledgement is also for Gregorio Mattiazzo for the English revision of this work and the encouragements during these last months.

Ringraziamenti speciali e particolari vanno a tutti i miei amici, vicini e lontani, d'infanzia e di studio, che mi hanno sostenuto in questi anni da studente. In particolare, ringrazio Daniele Calzolari per avermi accompagnato durante il lungo viaggio che dall'ombra della torre ci ha portati fin qui in terra d'Olanda. Un grazie speciale va poi a tutti i miei familiari che mi hanno incoraggiato in tutti questi anni. Ma il più importante ringraziamento è riservato a Gianfranco, Mariella, Daniele e Marco per avermi supportato, sopportato e finanziato in questi sette lunghi anni. Grazie per l'affetto, la disponibilità e la comprensione che in ogni momento avete saputo darmi.

Tot slot wil ik ook alle broeders en zusters van de gemeenschappen van de Neokatecumenale Weg in Nederland danken want bij jullie heb ik een familie gevonden. In het bijzonder ben ik de broeders en zusters van de eerste gemeenschap van Den Haag dankbaar. Dank u wel voor jullie gebeden en voor de liefde die jullie mij getoond hebben.

ABSTRACT

The wind speed profile in a marine environment is investigated using the data provided from the German offshore research platform FINO-1 and the meteorological mast of the Dutch offshore wind park Egmond aan Zee. The data are compared to the Monin-Obukhov Similarity Theory using the Richardson Bulk Method, the Richardson Gradient Method and the Profile Methods. The results show that the models do not predict the wind speed profile well especially for stable stratifications and large scatter is present. Each model shows different ways to estimate the wind speed profile. The Richardson Bulk Method provides more accurate estimations as compared to other methods and thus it is preferred in further analyses. A sensitivity study is conducted for the model input parameters. The effects of sea surface and air temperatures, coast distance (fetch), reference wind speed and surface boundary layer height are analyzed in terms of mean wind speed estimation and its standard deviation. The model is indeed sensitive to those parameters, especially to air temperature and surface boundary layer height. The use of satellite model database for offshore wind energy purposes is shown in the last part of this work. The weather forecast model COSMO-EU, stored in the database of the Deutscher Wetterdienst DWD, is analyzed consequently and the data are compared with the measurements of FINO-1 for validation. Combinations of real and estimated measurements, respectively from FINO-1 and DWD, are shown for sea surface and air temperatures and relative humidity.

TABLE OF CONTENTS

List of Figures

List of Tables

Nomenclature

Symbol	**Description**
C	Coefficient for the Richardson Bulk Method
C_1	Coefficient for the Richardson Bulk Method
c_p	Specific heat
DALR	Dry adiabatic lapse rate
Es	Saturation vapour pressure
f_c	Corioli coefficient
g	Acceleration of gravity
k	von Karman constant
ki	Coefficient that relates z_i to u_*
L	Obukhov length
lat	Latitude
L_v	Latent heat of vaporization
M	Molar mass of air
ni	Coefficient that relates z_s to z_i
P	Air pressure
P_0	Reference air pressure
q	Kinematic heat flux
r	Sample correlation coefficient
R	Constant of perfect gas
R_{air}	Gas constant for dry air
RH	Relative humidity
Ri_b	Bulk Richardson number
Ri_Δ	Gradient Richardson number
T	Absolute air temperature
T'	Fluctuation of temperature

T_0	Generic surface temperature
$T_{air\text{-}sea}$	Temperature at the interface air-seawater
T_D	Dew temperature
T_m	Submerge seawater temperature
T_{sea}	Absolute temperature at the interface air-seawater
T_v	Virtual air temperature
Tv_{sea}	Virtual temperature at the interface air-seawater
$\overline{u}$	Mean value of the horizontal wind speed component
u	Average wind speed in the horizontal direction
U	West-East wind speed component in DWD database
u'	Instantaneous wind speed in the horizontal direction
u_*	Friction velocity
u_1	Wind speed measured at z_1
u_2	Wind speed measured at z_2
v	Average wind speed in the lateral direction
V	South-North wind speed component in DWD database
v'	Instantaneous wind speed in the lateral direction
w	Average wind speed in the vertical direction
w'	Instantaneous wind speed in the vertical direction
X	Upwind distance to the coast
Y	Downwind distance to the coast
z	Vertical coordinate
z'	Level at which Ri_Δ is valid
z_0	Roughness length
z_1	Lower level at which the wind speed is measured
z_2	Higher level at which the wind speed is measured
z_i	Planetary boundary layer height
z_{ref}	Reference level
z_s	Surface boundary layer height
z_t	Roughness length for temperature
α	Charnock's coefficient
ε_a	Ratio of gas constant for dry air to moist air

ζ	Stability dimensionless parameter equals to z/L
θ	Potential temperature
θ_*	Temperature scale
θ_{*v}	Virtual temperature scale
θ_v	Virtual potential temperature
θ_{v1}	Virtual potential temperature at z_1
θ_{v2}	Virtual potential temperature at z_2
$\theta v_{air\text{-}sea}$	Virtual potential temperature at air-seawater interface
ρ	Air density
ϕ_m	Universal non-dimensional function for the wind speed
ϕ_t	Universal non-dimensional function for the temperature
Ψ_m	Integrated function of ϕ_m
Ψ_t	Integrated function of ϕ_t

Acronyms

Acronym	Description
BSH	Bundesamt für Seeschifffahrt und Hydrographie
CFD	Computational Fluid Dynamics
DWD	Deutscher Wetterdienst
GL	Germanischer Lloyd
GME	Global weather forecast model
MO	Monin-Obukhov Similarity Theory
NWP	Numerical Weather Prediction
PBL	Planetary Boundary Layer
Ri_{bulk}	Richardson Bulk Method
$Ri_{gradient}$	Richardson Gradient Method
SST	Sea Surface Temperature
STD	Standard Deviation
T_{diff}	Temperature Difference Profile Method
T_{sea}	Sea Temperature Profile Method
$U_{diff}T_{diff}$	Wind speed and Temperature Difference Profile Method
UTC	Universal Time Coordinate

Chapter 1

INTRODUCTION

The offshore wind energy is gaining more and more importance in the scenario of the European renewable energies. Due to high costs of installation and maintenance, it is important to have a good assessment of the wind speed profile. The wind speed at the turbine hub level is used in the assessment of the energy yield and the knowledge of the wind shear helps estimating the turbine structure loads (for example stress fatigue of the blades).

In the last few years a lot of companies and institutes have spent money and interest in the investigation of the wind field over sea surface highlighting the differences with respect to onshore conditions. Several parameters influence the wind offshore: the distance from the shore (fetch), the stability of the atmosphere, the waves and currents. In the last years, according to different authors, a theory developed for the flow above canopy in the ‘50s by the Russian A. S. Monin and A. M. Obukhov has been used to describe the offshore wind speed profile. Several researches have been conducted, especially in the Baltic Sea, to validate this theory. Many of these works have been conducted using measurements close to the coast and with a short meteorological mast (only up to 50m). The results from these experimental campaigns do not show consistent results but rather considerable errors in the wind speed prediction. However, nowadays, this theory is applied more and more for offshore wind profile estimation. Furthermore in literature different results have been obtained treating the data differently and using dissimilar definitions of important model parameters.

The aim of this work is, hence, to provide an insight into the Monin-Obukhov Similarity Theory for the North Sea, using two significant offshore databases and one weather forecast model database. The offshore databases are the German research platform FINO-1 located at about 45 km from the coast and the meteorological mast of the first Dutch offshore wind farm

Egmond aan Zee at about 18 km from the shore. The weather forecast model is the COSMO-EU run in the computers of the German National Weather Forecast (Deutscher Wetterdienst, DWD). Five variants of the theory are applied to these offshore databases, a sensitivity study and a comparison between real data and weather model are conducted. The goal of this study is to validate wind shear offshore using various datasets and coupling it with the previous researches about this topic.

The work is divided in five chapters explaining the different aspects of the problem. Chapter 2 explains the assumptions and equations of the Monin-Obukhov Similarity Theory and of the five variants treated. Further an overview of COSMO-EU model is given. Chapter 3 provides an insight into the three aforementioned databases. In Chapter 4 the results of the five model variants are compared with the measurements of the two offshore sites FINO-1 and Egmond aan Zee. Chapter 5 treats the sensitivity study of several input parameters of the Monin-Obukhov Similarity Theory. Chapter 6 investigates the DWD database and compares it with the data of the platform FINO-1. Few conclusions and recommendations are given in Chapter 7.

Chapter 2

THE MODELS

The wind speed profile of the atmospheric boundary layer (PBL) cannot be easily assessed due to many parameters influencing the phenomenon. The air can be regarded as a Newtonian fluid and modelled by means of the Navier-Stokes equations. The most common relation comes from the Navier-Stokes equation for the turbulence kinetic energy TKE (see Chapter 5 of [1]), where TKE is the sum of the average square fluctuations of the wind velocity ($TKE = 0.5 \cdot (\overline{u'^2} + \overline{v'^2} + \overline{w'^2})$). In this relation several terms contribute to the definition of TKE (buoyancy, dissipation, etc.). All these terms have been divided by u_*^3/kz to make the relation non dimensional.

$$\frac{kz}{u_*} \cdot \frac{\partial \overline{u}}{\partial z} = \phi_m \tag{2.1}$$

The left hand side of equation (2.1) represents the mechanical or shear production/loss term in the non-dimensional TKE equation. If the other terms are included altogether in the right hand side, equation (2.1) shows that the wind speed gradient can be written as a function of an appropriate non-dimensional universal function ϕ_m and that is proportional to the friction velocity u_* (as defined in (2.2) for appropriate system of reference, with *u'* and *w'* the wind speed fluctuations respectively parallel and perpendicular to the average of the main wind speed component $\overline{u}$), k the von Karman constant (normally equals to 0.4) and the reference level z.

$$u_*^2 = \left| \overline{u'w'} \right| \tag{2.2}$$

When it is possible to assume that the mechanical wind shear term is in equilibrium with the buoyancy term (i.e. the effects compensate), the universal function ϕ_M is obviously equals to

1. Hence, for these conditions, equation (2.1) can be rewritten as in (2.3) and integrating its both sides between the roughness length z_0 (i.e. the height above ground for which the wind speed is assumed equal to zero, see [2] and [3]) and the reference height z_{ref}, as shown in equation (2.4).

$$\partial \overline{u} = \frac{u_*}{kz} \partial z \tag{2.3}$$

$$\int_0^{u_{ref}} du = \int_{z_0}^{z_{ref}} \frac{u_*}{kz} dz \tag{2.4}$$

Solving equation (2.4) and considering a general level z and wind speed u, the logarithmic wind speed profile is found. This relation is valid only for near-neutral conditions, i.e. when ϕ_M is 1.

$$u(z) = \frac{u_*}{k} \ln\left(\frac{z}{z_0}\right) \tag{2.5}$$

For general conditions, the universal function ϕ_M is not 1 and the derivation of the wind speed profile is more complex. A specific universal function that takes into account the values of the other terms (like buoyancy and dissipation) in the TKE equation is needed.

This necessity is overcome via the Monin-Obukhov Similarity Theory (MO)[1]. This theory (valid only within the lower part of the atmospheric boundary layer and for stationary conditions) was developed in 1954 by A. S. Monin and A. M. Obukhov [4], describing the wind speed profile above the canopy. They assumed, according to Buckingham's Π-theorem, that the parameters g/T_0 (with T_0 the surface temperature), u_*, and $q/(c_p \cdot \rho)$, (q being the kinematic heat flux, c_p the specific heat and ρ air density), describe the atmospheric turbulence above the canopy. Only one parameter with the dimension of length is possible to describe these processes, the Obukhov Length L (equation (2.6)).

[1] Similarity theory is an empirical method of finding universal relationships between variables that are made dimensionless using appropriate scaling factors.

$$L = -\frac{u_*^3}{k\,\frac{g}{T_0}\cdot\overline{w'T'}} \tag{2.6}$$

In the surface layer (Prandtl-layer, constant flux layer), the vertical fluxes were assumed to be constant with the elevation and *T'* and *w'* represent the fluctuations of temperature and vertical wind velocity. *L* is an index of the surface atmospheric stability and indicates how the heat and momentum exchanges influence the wind shear. From Buckingham's Π-theorem, the universal function of the wind speed gradient should be only a function of the dimensionless parameter $\zeta = z/L$ and similar for the temperature gradient; thus equations (2.7) and (2.8) are found.

$$\frac{kz}{u_*}\cdot\frac{\partial\overline{u}}{\partial z} = \phi_m\left(\frac{z}{L}\right) \tag{2.7}$$

$$\frac{z}{T_*}\cdot\frac{\partial\overline{T}}{\partial z} = \phi_t\left(\frac{z}{L}\right) \tag{2.8}$$

Hence, integrating these two equations the expressions for wind speed and potential temperature profile are found.

$$u(z) = \frac{u_*}{k}\left[\ln\left(\frac{z}{z_0}\right) - \Psi_m\left(\frac{z}{L}\right)\right] \tag{2.9}$$

$$\theta(z) = \theta(z_t) + \frac{\theta_*}{k}\left[\ln\left(\frac{z}{z_t}\right) - \Psi_t\left(\frac{z}{L}\right)\right] \tag{2.10}$$

In these equations, Ψ_m and Ψ_t are universal functions for wind speed and temperature respectively, θ_* is the temperature scale and z_t is the surface roughness length for temperature. The most used universal function (especially for wind energy applications) is the Businger-Dyer for wind speed and temperature profiles, as suggested in [5]:

$$\Psi_m\left(\frac{z}{L}\right) = \Psi_t\left(\frac{z}{L}\right) = -\frac{5z}{L} \tag{2.11}$$

$$\Psi_m\left(\frac{z}{L}\right) = 2\ln\left[\frac{(1+x)}{2}\right] + \ln\left[\frac{(1+x^2)}{2}\right] - 2\tan^{-1}(x) + \frac{\pi}{2}$$

$$\Psi_t\left(\frac{z}{L}\right) = 2\ln\left[\frac{(1+x^2)}{2}\right] \tag{2.12}$$

$$x = [1-(16 \cdot z/L)]^{1/4}$$

$$\Psi_m\left(\frac{z}{L}\right) = \Psi_t\left(\frac{z}{L}\right) = 0 \tag{2.13}$$

Equation (2.11) is valid for stable conditions, while for unstable and near-neutral conditions equations (2.12) and equation (2.13) hold respectively. The airflow varies under different atmospheric stratifications due to the different roles played by the momentum and heat fluxes. Hence, as function of stability, the wind speed profile assumes different shapes. For this reason it is important to distinguish between stable, unstable and near-neutral atmospheric stratifications and to provide different equations.

The stability of the atmosphere is basically determined by comparing the lapse rate of an air parcel to the lapse rate of the surrounding air, i.e. environment. A stable atmosphere is the one strongly resistant to change. If some external force, such as orographic lifting or convergence pushes the air upward, the temperature of the rising air relative to the environment suggests that the air would rather return to its original position. In a stable atmosphere, if one lifts a parcel of air, the temperature of the rising air will decrease rapidly so that its temperature will always be colder than the temperature of the environment. Colder air sinks. If the force pushing the air up suddenly disappeared, the parcel would sink back to its original position where its temperature and pressure would be in equilibrium with the environment. Another way of stating that the atmosphere, or a layer in the atmosphere, is stable means that the lapse rate of the rising air is greater than the lapse rate of the environment. (Note: A positive lapse rate indicates a decrease in temperature with height.) A layer characterized by a temperature inversion, defined by a negative lapse rate, is considered extremely stable. These inversions near the surface often occur in the early morning hours before sunrise. Normally stable stratifications occur when warm air flows over cold surfaces. In a neutral atmosphere (or near-neutral) the temperature lapse rates of air parcel and environment are equal. If a parcel of air is lifted through a neutral layer, the temperature and pressure of the parcel will be identical to the temperature and pressure of the surrounding air at every level and it is always in equilibrium with the environment. If the force producing the motion ceases, the parcel will neither continue to rise nor begin to sink, rather, the motion of a parcel will also cease. At times, in the atmosphere, a little push goes a long way. If a parcel of air is lifted and continues to rise after the lifting force disappears, the atmosphere is unstable. In an unstable layer, the lapse rate of a rising parcel is less than the lapse rate of the environment.

The Obukhov length *L* is the parameter used to define atmospheric stability. The stability is usually classified in five classes, according to [6], as reported in Table 2.1. The use of classes helps to understand the different wind profiles with respect to the stability of the atmosphere. The non-dimensional parameter $\zeta = z/L$ is positive for stable conditions, negative for unstable and almost zero for near-neutral conditions.

Stability Class	Range
Very stable	0 < L < 200 m
Stable	200 < L < 1000 m
Near-neutral	|L| > 1000 m
Unstable	-1000 < L < -200 m
Very unstable	-200 < L < 0 m

Table 2.1: Stability Classification

The estimation of *L* is thus the most important element in the definition of the wind speed profile (according to MO) but it is not straightforward. There are different methods proposed in literature and three will be treated and used to analyse two datasets presented in this work.

The theory proposed until now is valid both for onshore and offshore. The difference between them (assuming MO valid for surfaces other than canopy) is only in the definition of the roughness length. In onshore fields, the roughness length is constant and depends on the characteristics of the terrain. Offshore, instead, it is related to the height and the shape of the waves, which varies. When the wind blows over the sea, the roughness depends on the wind speed itself. The shear between the fluids (water and air) creates the movement of the water and the wave's origin. The height of the waves is a function of many factors, but the most important are the surface wind speed, the upstream and downstream distance from the coast and the sea depth. This gives difficulties in modelling the roughness parameter. In literature many works can be found on this topic and different models have been created and tested, however the differences in the results are small (see [7], [8], [9] and [11]). The most common model is the Charnock's equation [12]. It takes into account the wave field considering its dependence on friction velocity u_* as shown in equation (2.14):

$$z_0 = \alpha \frac{u_*^2}{g} \tag{2.14}$$

where α is the Charnock's coefficient, g the acceleration of gravity and u_* is the friction velocity. This formulation is a common parametric characterisation of the aerodynamic roughness length over water, which does not explicitly incorporate information on wave state. It assumes that the wave state influence on the roughness length is represented by surface stresses. α is an empirical value and it is site dependent. It is therefore advisable to compute its value for every site rather than take a reference value. The Charnock's equation can be in this way tuned by means of its parameter α. Rearranging equation (2.9) as a function of u_* and substituting it into (2.14), it is possible to find the equation that links directly the z_0 and the mean wind speed;

$$z_0 = \frac{\alpha}{g}\left[\frac{u \cdot k}{\ln(z/z_0) - \Psi_m(z/L)}\right]^2 \tag{2.15}$$

in which u is the wind speed measured at the reference elevation z. Since it is not possible to know in advance the suitable value of the Charnock's coefficient for each site, the value of 0.011 is recommended in the standards [13]. However in this work the value of 0.0144 has been used according to references [5] and [14].

Methods to estimate L are shown in the following sections of this chapter. They are: Richardson Bulk (Ri_{bulk}) Method, Richardson Gradient ($Ri_{gradient}$) Method and Profile Method. The Profile Method has three variants: Sea Temperature (T_{sea}) Profile Method, Temperature Difference (T_{diff}) Profile Method, Wind Speed and Temperature Difference ($U_{diff}T_{diff}$) Profile Method. The last section describes the weather forecast model COSMO-EU.

2.1 Richardson Bulk Method

Air and sea temperature measurements are used together with the wind speed at a certain elevation. An approximation method suggested by Grachev and Fairall [15] is proposed. The dimensionless stability parameter ζ is proportional to the bulk Richardson number Ri_b according to equation (2.16) for $Ri_b < 0$ and to equation (2.17) for $0 < Ri_b < 0.2$. The model does not work for values of Ri_b larger than 0.2. The coefficients C and C_1 can be found in literature and they offer different values. Respectively the values of 10 and 5 are suggested in [15].

$$\zeta = CRi_b \tag{2.16}$$

$$\zeta = \frac{CRi_b}{1 - C_1 Ri_b} \tag{2.17}$$

$$Ri_b = -\frac{g}{\theta_v}\frac{z\Delta\theta_v}{u^2} \tag{2.18}$$

$\Delta\theta_v$ indicates the virtual potential temperature difference between reference level z and sea surface level. The variables needed for this computation are the air virtual potential temperature θ_v at z, the air virtual potential temperature $\theta_{v\ air\text{-}sea}$ at the air-sea interface and the wind speed u. The wind speed u is regarded as reference wind speed, while the predicted wind speed at higher levels is called u_{pred}. u_{pred} is then compared to the highest level wind speed u_{meas} of the met masts (90m in FINO-1 and 116m in Egmond aan Zee). The air virtual potential temperature θ_v derives from the absolute temperature T in which the pressure P (potential) and the relative humidity RH (virtual) are taken into account. When only P is considered the potential temperature θ is found. Similar, with RH the virtual temperature T_v is found. Air temperature from the measurements is always the absolute temperature and labelled T.

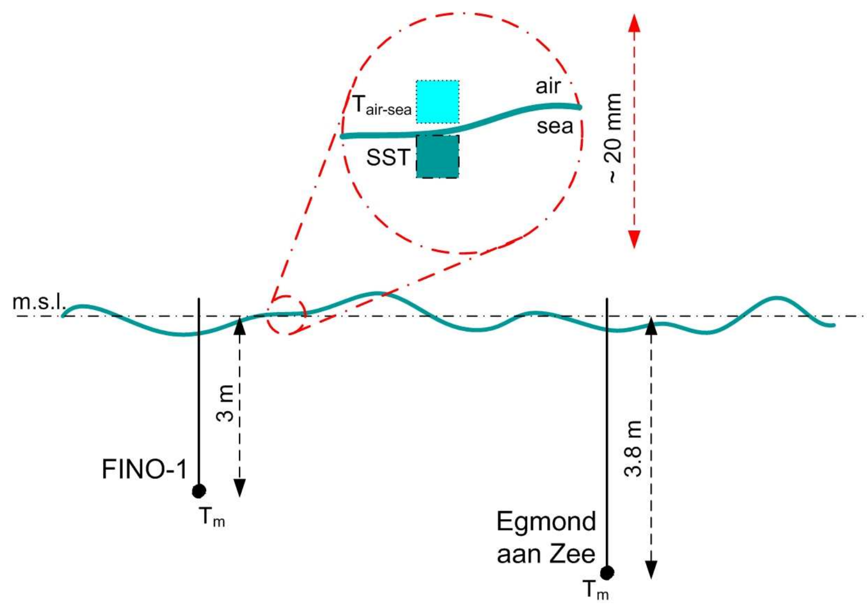

Figure 2.1: Sea surface temperature and submerging sensor position in FINO-1 and Egmond aan Zee.

The situation is complex when $\theta_{v\ air\text{-}sea}$ has to be defined. Figure 2.1 shows how the sea temperature is measured in FINO-1 and Egmond aan Zee. The absolute temperatures (T_m) are taken at 3m below the mean sea level for FINO-1 and 3.8m for Egmond aan Zee. These temperatures are supposed to be the respective equivalent SST, which is the absolute temperature of the particles (where particle can be defined as a small volume with the same characteristic of pressure, density and temperature) at the air-sea interface. In other words, T_m is equivalent to SST and hence equals to $T_{air\text{-}sea}$. With these assumptions the effects of the temperature gradient within the seawater, the cool-skin and warm-layer effects [16] are neglected. $T_{air\text{-}sea}$ is converted into the virtual temperature Tv_{sea} assuming a RH of 100%. Since Tv_{sea} is at the sea level, it corresponds to the potential virtual temperature because the pressure is equal to the reference P_0. Thus the temperature used in the Ri_{bulk} Method is Tv_{sea} and $\Delta\theta_v$ is expressed in (2.19).

$$\Delta\theta_v = Tv_{sea} - \theta_v \tag{2.19}$$

The results with both virtual and absolute $T_{air\text{-}sea}$ are shown in Chapter 5; in this case the absolute sea surface temperature is labelled T_{sea}. A distinction is made between measured sea surface temperature and value used as input for the models. The sea surface temperature is always labelled as *SST* when the value of the measurement is considered (and it is always intended as the temperature value of the seawater particle). This is because in the two offshore databases the submerging temperature T_m is assumed to be *SST* while DWD database provides the "real" value of *SST*. The sea surface temperature value (i.e. the temperature value of the air particle) used for the calculations is always labelled as Tv_{sea} or T_{sea} (virtual or absolute).

2.2 Richardson Gradient Method

Temperature and wind speed difference at two elevations are used to estimate the gradient Richardson number Ri_Δ ([7],[10] and [11]):

$$Ri_\Delta(z') = \frac{(g/\theta_v)(\Delta\theta_v/\Delta z)}{(\Delta u/\Delta z)^2} \tag{2.20}$$

The term $\Delta\theta_v/\Delta z$ is the potential virtual temperature difference at a specific vertical elevation difference. All the differences are taken with the first measurement lower than the second, as expressed in (2.21).

$$\Delta z = z_1 - z_2 \tag{2.21}$$

Equally, $\Delta u/\Delta z$ is the wind speed difference at a specific vertical elevation difference. The height *z'*, at which Ri_Δ is valid, can be estimated, according to reference [8], as reported in (2.22).

$$z' = \frac{(z_1 - z_2)}{\ln(z_1 / z_2)} \tag{2.22}$$

The Ri_Δ is converted to L by means of equations (2.23):

$$L = \begin{cases} \dfrac{z'}{Ri_\Delta}, Ri_\Delta \le 0 \\ \dfrac{z'(1-5Ri_\Delta)}{Ri_\Delta}, 0 < Ri_\Delta < 0.2 \end{cases} \tag{2.23}$$

it means that for Ri_Δ higher than 0.2 the model loses validity, thus those values have to be excluded in the computation.

2.3 Profile Methods

Using the gradients of u, θ and humidity, it is possible to construct methods that do not use direct formulas to estimate L but an iterative process. Three different profile methods are presented in this work and they differ slightly for the definition of u_* and the virtual temperature scale θ_{*v}. The whole procedure suggested in this work is deeply explained in [5].

The method begins giving the initial values of L and z_0 respectively -1e^6 and 0.0002. Knowing these two values the universal functions for the wind speed (Ψ_m) and the temperature (Ψ_t) profiles can be found using the relationships for stable (2.11), unstable (2.12) and near-neutral (2.13) conditions. For even more stable conditions ($z/L > 0.5$) the universal functions are equal and it holds equation (2.24), suggested in [5]:

$$\Psi_m\left(\frac{z}{L}\right) = -0.7\frac{z}{L} - \left\{0.75\left(\frac{z}{L}\right) - 10.72e^{(-0.35(z/L))}\right\} - 10.72 \tag{2.24}$$

At this step, knowing Ψ_m and Ψ_t, u_* and θ_{*v} can be calculated using the three methods proposed: T_{sea} *Profile Method* [5], T_{diff} *Profile Method* [14] and $U_{diff}T_{diff}$ *Profile Method* [17].

2.3.1 Sea Temperature Profile Method

The measurements used with this method are: *u*, *SST*, *T* and *RH*. Generally *u* and *T* can be measured at different levels but in this paper they are taken at the same elevation *z*. *RH* is measured at *z* and used to avoid the humidity universal function in the computation. This means that θ_v is used instead of *T*. *SST* is used to calculated the Tv_{sea} (with the assumption of 100% of *RH*, as explained in section 2.1).

u_* and θ_{*v} are calculated using relation (2.25) and relation (2.26) respectively.

$$u_* = \frac{u(z)\cdot k}{\left[\ln\left(\frac{z}{z_0}\right) - \Psi_m\left(\frac{z}{L}\right)\right]} \tag{2.25}$$

$$\theta_{*v} = \frac{\left(\theta_v - Tv_{sea}\right)\cdot k}{\left[\ln\left(\frac{z}{z_t}\right) - \Psi_t\left(\frac{z}{L}\right)\right]} \tag{2.26}$$

Where z_t is the roughness length for temperature and it is function of stability in the form expressed in (2.27).

$$\begin{aligned} z_t &= 2.2\times10^{-9},\ for(z/L > 0) \\ z_t &= 4.9\times10^{-5},\ for(z/L < 0) \end{aligned} \tag{2.27}$$

2.3.2 Temperature Difference Profile Method

The measurements used with this method are: u at one level and two air temperatures at two different levels. In this work u and T are taken at the same level z_1 and the other T at higher-level z_2. Further RH is measured at z_1 and z_2. u_* and θ_{*v} are calculated using relations (2.28) and (2.29) respectively.

$$u_* = \frac{u_1 \cdot k}{\left[\ln\left(\frac{z_1}{z_0}\right) - \Psi_m\left(\frac{z_1}{L}\right)\right]} \tag{2.28}$$

$$\theta_{*v} = \frac{(\theta_{2v} - \theta_{1v}) \cdot k}{\left[\ln\left(\frac{z_2}{z_1}\right) - \Psi_t\left(\frac{z_2}{L}\right) + \Psi_t\left(\frac{z_1}{L}\right)\right]} \tag{2.29}$$

2.3.3 Wind Speed and Temperature Difference Profile Method

In this last method the measurements are wind speeds and air temperatures at different elevations. The wind speeds and temperatures are taken at the same two levels z_1 and z_2. RH is measured at z_1 and z_2. u_* and θ_{*v} are calculated using equations (2.30) and (2.31) respectively.

$$u_* = \frac{(u_2 - u_1) \cdot k}{\left[\ln\left(\frac{z_2}{z_1}\right) - \Psi_m\left(\frac{z_2}{L}\right) + \Psi_m\left(\frac{z_1}{L}\right)\right]} \tag{2.30}$$

$$\theta_{*v} = \frac{(\theta_{2v} - \theta_{1v}) \cdot k}{\left[\ln\left(\frac{z_2}{z_1}\right) - \Psi_t\left(\frac{z_2}{L}\right) + \Psi_t\left(\frac{z_1}{L}\right)\right]} \tag{2.31}$$

With the values of the u_*, the roughness length z_0 is calculated using the Charnock's equation (2.14). Using the calculated u_* and θ_{*v}, the new L is estimated (2.32).

$$L = \frac{(u_*)^2 \theta_v}{kg\theta_{*v}} \tag{2.32}$$

This new value of L and the new z_0 are then used as starting points to compute the values of Ψ_m and Ψ_t and so, the new u_* and θ_{*v}. The iterative routine ends when the change in L is less than 5% or when the number of iterations exceeds 10. The value of L and the last value of z_0 are thus utilised to estimate the values of wind speed at higher elevations (u_{pred} and u_{meas} are respectively predicted and measured u at the highest anemometer level).

2.4 Weather Forecast Model COSMO-EU

The last part of this work focuses on the capability to describe the wind profile offshore using data obtained by a weather forecast model. To achieve this goal, a research is done looking for the most suitable model in the region of the North Sea and the COSMO-EU weather forecast model [18], provided by DWD (Deutscher Wetterdienst), has been chosen for its wealth of data (wind and sea state) and its fineness of the grid points.

COSMO-EU is a subdivision of a global weather forecast model (GME). GME is the first operational weather forecast model that uses an icosahedral-hexagonal grid covering the globe. This grid structure offers the advantage of a rather small variability of the area of the grid elements. The macro-triangulation of the GME grid is based on an icosahedron on the surface of a sphere. Two of the twelve vertices of the icosahedron coincide with the north and south poles. Connecting the twelve vertices by great circle arcs, 20 triangles on a sphere (non-Euclidean) are formed with an edge length of 7054 km (see Figure 2.2). By iteratively sub-dividing these large triangles into smaller ones, a grid of the required resolution can be derived.

Figure 2.2: Structure of GME grid, first icosahedron with 20 faces [19].

The grid spacing of the resulting grid is defined as the mean edge length of the smallest triangles; currently the grid spacing of GME is 40 km. The vertices of the triangles, which form the grid points, are surrounded by six (five at the 12 special points of the original icosahedron) triangles. The grid points are therefore the centres of these hexagons or pentagons. The GME grid approximates the sphere by 368630 hexagons (grid spacing of 40 km) and 12 pentagons. The mean size of a grid element is thus 1384 km^2. All model variables are defined as mean values over the area of a grid element.

The main variables of GME are surface pressure, horizontal wind components, temperature, specific contents of water vapour, cloud water and cloud ice and ozone in 40 layers of the atmosphere, from the surface up to a height of approximately 31 km.

The observations used as input to the GME model are:

- land stations and ships (surface pressure, temperature and humidity at 2 m as well as horizontal wind speed and direction at 10 m above the ground)
- buoys (surface pressure, horizontal wind speed and direction at 10 m above the sea surface)
- radiosondes (vertical profiles of wind, temperature and humidity)
- aircrafts (wind, temperature)
- vertical sounders on polar-orbiting satellites (temperature)
- geostationary satellites (wind state from sequences of satellite images)

The outputs from the GME model are then used as boundary conditions for the regional model COSMO-EU (i.e. the model with finer grid and simulation timing for the Europe).

COSMO is one of the first operational Numerical Weather Prediction (NWP) models worldwide based on the full Euler equations without any scale-dependent approximations. Such non-hydrostatic models solve, contrary to traditional hydrostatic models like GME, a prognostic (predicted) equation for the vertical velocity. Non-hydrostatic models could in principle use extremely small grid spacing, e.g. 100 m, while hydrostatic models are restricted to grid spacing larger than 10 km, i.e. to scales where vertical accelerations are small compared to horizontal accelerations. The non-hydrostatic equations describe the atmosphere by the same kind of equations which are used in general fluid dynamics, without using special approximations for meteorological flows, which commonly are used for large-scale atmospheric flows. The application COSMO-EU (COSMO Europe) covers the Eastern Atlantic and Europe with 665 x 657 = 436905 grid points at a grid resolution of 7 km. The model has a rectangular grid instead of triangular ones as for GME and it has 40 layers in the atmosphere from the surface up to a height of approximately 24 km. Therefore COSMO-EU resolves many local topographic details (like orography) which have an important influence on the local weather.

The atmospheric prognostic variables of COSMO-EU are pressure, horizontal and vertical wind components, temperature, specific contents of water vapour, cloud water and cloud ice, rain and snow, and turbulent kinetic energy. Over the oceans, the sea surface temperature (*SST*), analysed once a day, is kept constant throughout the forecast range. The *SST* is analysed at UTC 00 and changed at UTC 01, i.e. the data at UTC 00 is still the value of day before.

For the daily operational schedule of COSMO-EU it has to differentiate between the data assimilation and forecast suites (see Figure 2.3). The initial state of COSMO-EU forecast is based on a nudging analysis scheme, which allows assimilating continuously all observations available at high temporal resolution like surface-level, wind profiler or aircraft data. Eight times a day the forecast suite provides predictions of the weather up to 78 hours (based on the 00 and 12 UTC analyses), 48 hours (for 06 and 18 UTC) or 24 hours (for 03, 09, 15 and 21 UTC). COSMO-EU forecast fields are stored at hourly intervals.

The data in the assimilation scheme for the COSMO model is based on the nudging technique. This consists of subsisting supplementary correction terms in the forecast model equations during the forward integration of the model in time (with a time step of 40 seconds). Throughout the assimilation sequence, these terms relax the model state gently towards the observed values and thus ensure that the model develops in a way confirmed by the observations. The observations used in this nudging technique are listed below:

- land stations and ships (surface pressure, humidity at 2m and wind at 10 m above the ground; temperature observations at 2m height are currently used to derived information on the soil moisture rather than to influence directly the atmosphere in the model)
- buoys (surface pressure, wind at 10 m above the sea surface)
- radiosondes (vertical profiles of wind, temperature, and humidity)
- aircrafts (wind, temperature)
- wind profilers (vertical profiles of wind)

The research platform FINO-1 is included in the observation sources and it is considered as a ship by the model.

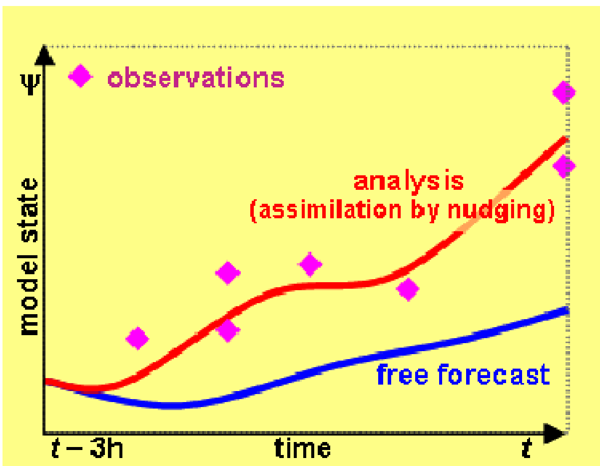

Figure 2.3: Analysis assimilation mode [19].

Even in the relatively fine-mesh grid of COSMO-EU it is not possible to simulate all small-scale processes directly. One example is the turbulent exchange of momentum, heat and water vapour between the ground and the lowest layers of the atmosphere. The related processes have typical dimensions of only a few meters. All these processes thus defy direct simulation in the model grid. In relation to the model grid they are sub-grid scale processes as opposed to the grid-scale processes that can be directly simulated. The scales of the parameterised processes are separate from those of the directly simulated processes that despite their small dimensions must not be neglected. Intensive interaction occurs in the atmosphere between all processes, even when they have completely different characteristic dimensions. This is why the sub-grid scale processes are also important for the correct simulation of the grid-scale processes in the NWP models. Therefore, they must not be neglected and taken into account by means of so-called parameterizations. The following processes are parameterized in the NWP models of the DWD:

- radiation
- grid-scale precipitation, cloud microphysics
- formation of showers and thunderstorms
- formation and dissolving of clouds
- turbulent exchange of momentum, sensible and latent heat between the earth's surface and the atmosphere
- sub-grid scale orographic effects (mainly from mountains)
- processes in the uppermost soil layers

Chapter 2

OFFSHORE DATABASES

Figure 3.1: FINO-1 and Egmond aan Zee, Google Earth® image.

In Figure 3.1 the locations of the two meteorological masts are shown using the satellite image of Google Earth®.

3.1 FINO-1

In connection with planned offshore wind farms, a research platform is set up in the North Sea to determine the possible effects of future offshore wind turbines on the marine flora and fauna. Germanischer Lloyd (GL) has been entrusted with coordinating the construction, erection, commissioning and operation of the platform. The research platform is funded by the Federal Ministry for the Environment, Nature Conservation and Nuclear Safety (BMU), here represented by the Jülich Research Centre (Project Management Organization Jülich, PTJ). The location of the research platform is about 45 kilometres north of the island of Borkum, with a water depth of about 30 metres (Borkum Riff, coordinates N 54° 0.86' E 6° 35.26', see Figure 3.1).

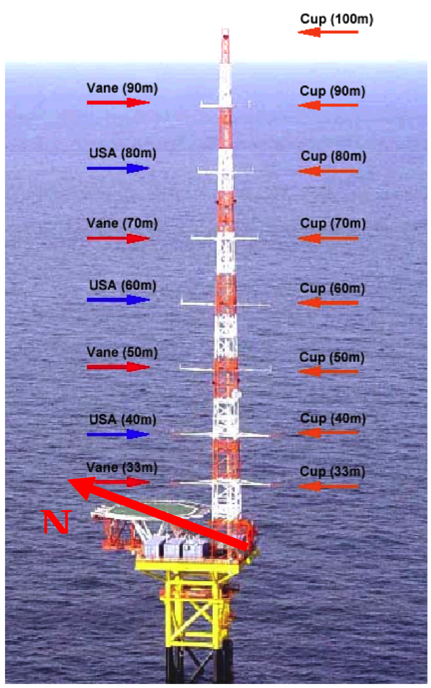

Figure 3.2: FINO-1 with indication of vanes and anemometers [20].

The level of the measurement mast is about 100m. Seven cup-anemometers are installed between levels of 30m and 100m on booms mounted in southeast direction of the mast (see Figure 3.2). A cup-anemometer is mounted at the top of the mast at about 103m from the m.s.l. Three ultrasonic anemometers are present at 40, 60, and 80m elevations. Additional meteorological measurements consist of *WD*, *T*, *RH*, *P* and solar irradiation. The oceanographic measurements include wave height, water current and physical properties of seawater.

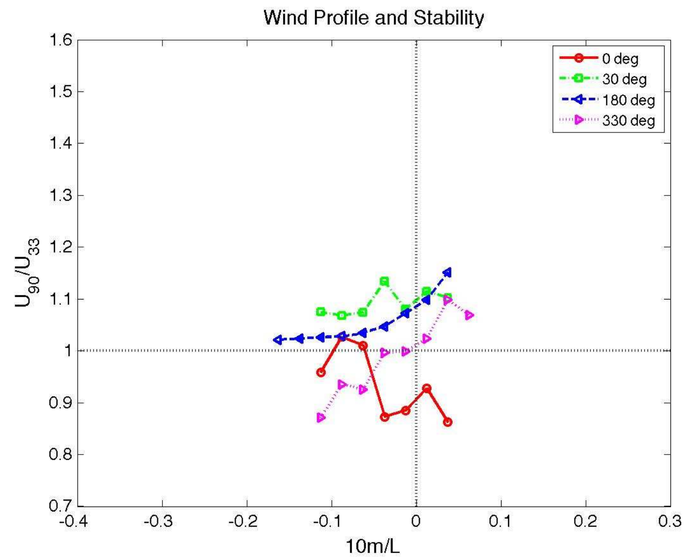

Figure 3.3: Wake effects of the structure in the research offshore platform FINO-1. The wind profile is subjected to the structure wake for the wind directions 0˚, 30˚ and 330˚N.

The data of the period 2004-2006 (except January 2004) are used for the analyses. The data of wind speed at 33, 50 and 90m elevations are used for the calculation; the wind direction (*WD*) is taken at 90m elevation, the temperature and relative humidity are taken at 30 and 50m; the sea temperature is taken at -3m and it is assumed to be the sea surface temperature (see Figure 2.1). The cup-anemometers (model A100LM of Vector Instruments, [21]) have a measurement error of ± 1% between 10.3 and 56.6 m/s wind speeds and ± 0.1 m/s below 10.3 m/s. The wind vane (model 4.3120.22.012 of Adolf Thies GmbH&Co.KG, [22]) has an accuracy of ± 2˚, with a resolution of 1˚. The air temperature and relative humidity are measured in a combined instrument (model 1.1005.50.512 of Adolf Thies GmbH&Co.KG, [22]) with the accuracy of ± 0.1˚ K for temperature and ± 3% of relative humidity. The sea temperature is measured by means of Pt 100 instrument (model 2.1280.00.000 of Adolf Thies GmbH&Co.KG, [22]) with an accuracy ± 0.1˚ K.

These measurements are provided by the online database [20]. All platform data can be downloaded from the website selecting sensor and period of interest. They are available as text files (.dat format). The available measurements are both validated and raw data. The validation is carried on by BSH (Bundesamt für Seeschifffahrt und Hydrographie) and consists of substituting erroneous measurement values with fixed ones, like -999 or 99.99. In this work, the validated date are used. However, these data contain still erroneous values especially with extremely high or low values of the measurements. The data with exactly the same wind speed at three different levels (33, 50 and 90m) are excluded because this indicates an error in measurement acquisition. The timeseries is not continuous, i.e. in the raw data many gaps can be found for which no values are present as well as from the BSH validation process. Hence the data have been selected excluding those fixed values, the extremely high or lower values and creating a continuous timeseries. Moreover several sensor outputs are stored in the database at different reference UTC time. Few minutes of delay were encountered between different time references. This complicates the use of the measurements. The data are thus arranged in a new timeseries in which all sensors have the same 10-min UTC reference time. This means that every hour six measurements are taken at minutes corresponding to 00, 10, 20, 30, 40 and 50. For example, one value with original reference time "2006-12-30 06:11:32" (year month day hour minutes seconds) is converted to "2006-12-30 06:10:00". In this way a consistent timeseries is constructed, which is easy to use for the analyses. The *WD* stored in the database has an offset of 45° because the wind vanes are aligned with the booms and not with the geographic North (see Figure 3.2). Hence the *WD* is corrected to indicate the geographic North. The data are not filtered for rapid change of values although these values are excluded when the stationary filter is applied in the analyses (see Chapter 4).

The data are also filtered for mast and platform structure shedding and the measurements within the sector 45˚N - 270˚N are used for this analysis. As it can be seen in Figure 3.3, the wind shear follows an expected path for the direction 180˚N while for the directions around North the structure modifies the airflow considerably and hence they have been excluded. The presence of the helipad influences the measurements between 0˚N and 30˚N, while the mast affects the measurements directly for *WD* of 330˚N. Although upwind the flow distortion produced by the mast can be considered linear, the effects of this error are not linear. However, these non-linear effects are small and, for the present analysis, they can be considered irrelevant. Thus, the effects of the mast upwind are small and they are considered equal for all levels except for the cup-anemometer at 103m that, indeed, is not used. The number of a 10-min mean value samples used for the analyses is about 40007 (excluding platform shadow, only wind speeds in the range 4-25 m/s at 90m elevation and only validated data) that correspond to 25% of availability in 3 years.

3.2 Egmond aan Zee

The second site considered is located at the first Dutch wind farm in front of the town Egmond aan Zee (see Figure 3.4). The met mast is shown in Figure 3.5 and it is located in WGS 84 coordinates at 52º 36’ 22.9’’ N and 4º 23’ 22.7’’ E at about 18 km from the coast. In Figure 3.5 the location of the meteorological mast is shown (the black cross surrounded by the red circle) with respect to the wind park. The picture shows that it is actually located close (about 300m) to the wind turbines and also that the wind turbines change the free stream wind speed.

The mast has a triangular lattice structure as shown in Figure 3.6 and all the sensors (anemometers, vanes, thermometers, humidity) are located at three different elevations: 21, 70 and 116m. The sea temperature sensor is located at 3.8m under the m.s.l. (see Figure 2.1). This measurement will be used in the models as *SST*. At each elevation the anemometers are located at the three corners (refer to Figure 3.6); in this way it is possible to extract the free stream according to *WD* reducing mast effects. The procedure to obtain the best wind direction is explained in details in [33]. The cup-anemometers (model 018 of Mierij Meteo, [24]) have an error of less than 0.5 m/s in the range 0.5 and 50 m/s. The wind vane (model 524 of Mierij Meteo, [24]) has an accuracy of about 0.7˚, with a resolution of 1.4˚. The air temperature and relative humidity are measured in a combined instrument (model HMP233 of VAISALA, [25]) with the accuracy of ± 0.1˚ K for temperature and ± 2% of relative humidity. The sea temperature is measured by means of Pt 100 instrument (model ST808 of Mierij Meteo, [24]) with an accuracy ± 0.1˚ K.

The measurements are available online through the database of the website [32]. All meteorological and sea data can be downloaded from the site selecting the month of interest. They are available as spreadsheets files (.xls format). The available measurements are validated data. The validation is carried on by NoordzeeWind [32] and consists of substituting erroneous measurement values with fixed ones, i.e. -99999. These data (as already explained for FINO-1) are excluded form the analysis. The data with exactly the same wind speed at three different levels (21, 70 and 116m) are excluded because this shows an error in data acquisition. The data are not filtered for rapid change of values but are filtered eventually with the stationary filter.

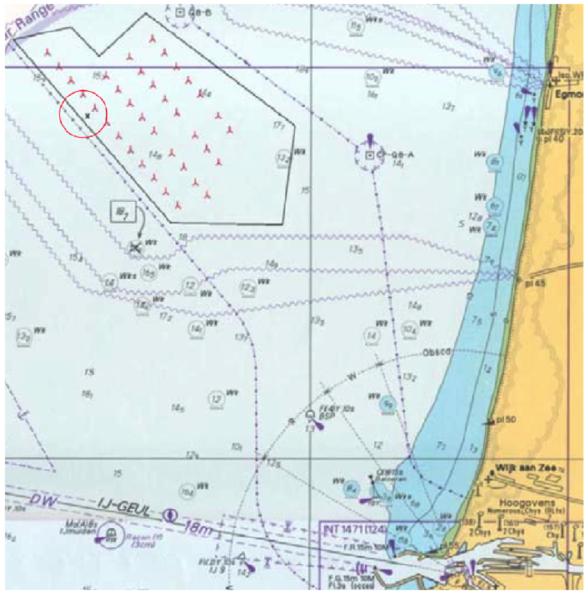

Figure 3.4: Egmond aan Zee wind park (black line) and met mast (red circle with black cross) [23].

Figure 3.5: Picture of Egmond aan Zee met mast.

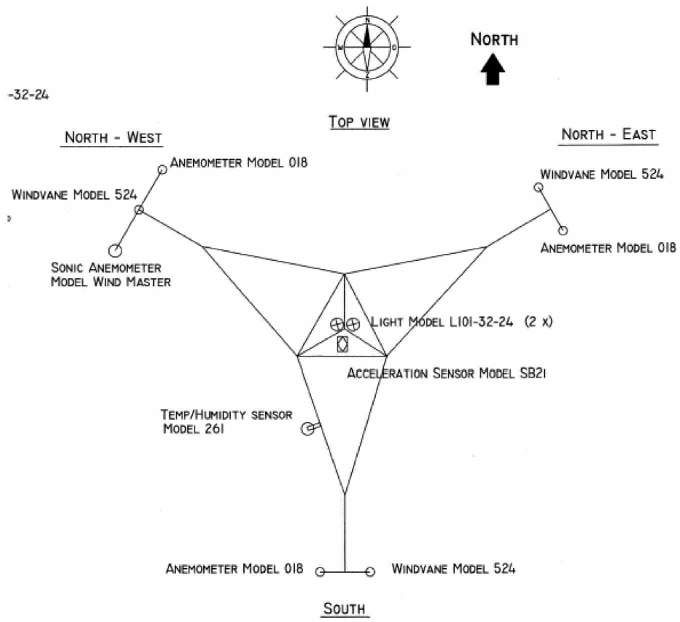

Figure 3.6: Sketch of the triangular lattice structure and anemometer locations in Egmond aan Zee [23].

The met mast was built in 2005 few months before the erection of the wind park. For that period all *WD* are undisturbed conditions. However, it is not easy to extract this information because the time of installation is not unique and the wind turbines within the park are not installed at the same time. All the available data have been filtered to avoid the measurements coming from the wind park and the only sector considered is 135˚ **-** 315˚ N. The period analysed here is from 01/07/2005 to 31/08/2008. Hence, the number of 10 minutes samples is about 62803 (excluding wind turbine wakes and only validated data), i.e. about 37% of the data.

3.3 Deutscher Wetterdienst

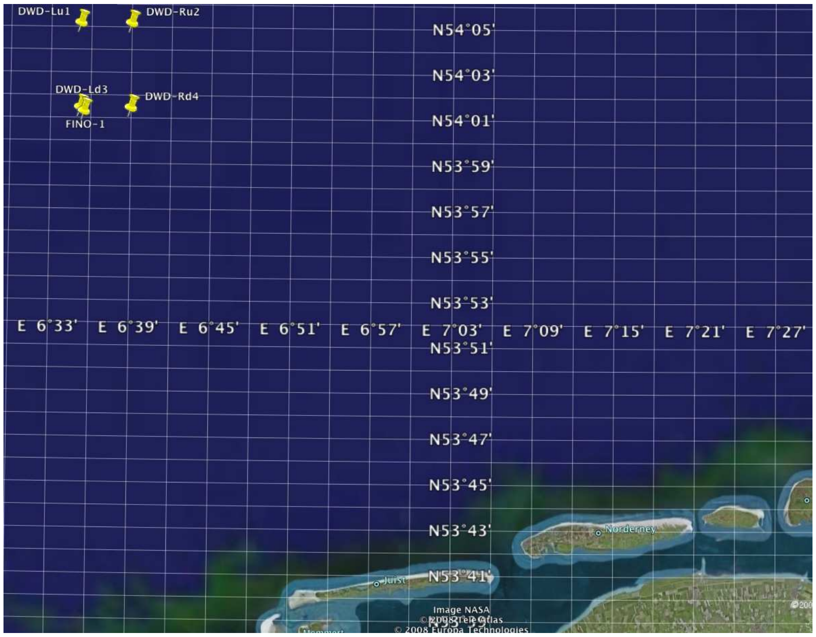

Figure 3.7: DWD data points at FINO-1 location, Google Earth® image.

Figure 3.7 shows the points nearby the research platform FINO-1 obtained thanks to German meteorological data centre DWD. The point labelled DWD-Ld3 is selected for this analysis because almost at the location of interest. The data come from the analysis-assimilation mode of COSMO-EU run in the supercomputer of DWD. The data are stored every hour using the assimilation mode explained in section 2.4. The data from the first guess are continuously corrected by nudging and the corrected values are stored in binary code (GRIB format). Any GRIB point corresponds to four grid points (the four corners of any cell) and, in this way, the closest point to FINO-1 has been selected. The four corners of the GRIB file obtained from DWD have got the coordinates shown in Table 3.1

For the analysis the following parameters, corresponding to the period 2005-2006 (i.e. 17023 1-hour samples available), have been selected from many others contained into the GRIB file:

- *P* at m.s.l.
- *SST*
- *T* and dew temperature at 2m above m.s.l.

- T, *U* and *V* at model layer levels of 10, 34.4, 68.8, 116.6 and 178.8m.
- *U* and *V* of wind speed at reconstructed 10m height.

The conversion of the parameters from GRIB format to dat format is provided by DWD itself. The data are already validated and the ones with -999.00 values are excluded from the analyses. The model has a fixed system of reference and *U* is the horizontal wind velocity component in the West-East direction and it is positive when the wind blows from West to East. *V* is the horizontal component in South-North direction and is positive when the wind blows from South to North. Hence, *u* and *WD* are derived from these two wind velocity components. The difference between model layer level and the reconstructed height is almost null over the oceans but it is consistent onshore because the land is not flat. In other words, the model reconstructs the wind speed at 10m knowing the orography of the specific place.

	Latitude	Longitude
DWD-Lu1	54.079˚ N	6.583˚ E
DWD-Ru2	54.079˚ N	6.646˚ E
DWD-Ld3	54.017˚ N	6.583˚ E
DWD-Rd4	54.017˚ N	6.646˚ E

Table 3.1: DWD grid point coordinates.

Chapter 4

RESULTS

In this chapter the results from measurements and MO theory are presented using the five models described in Chapter 2. The results are reported per method and for the two sites. Since the theory is valid only for stationary conditions and within the surface boundary layer height, in which u_* is assumed constant, filters have been applied to the samples. The results are presented with these filters and the differences are highlighted. The effects of the two filters are shown only for Ri_{bulk} Method.

The stationary filter excludes the values measured when the mean conditions of air and sea are changing rapidly so that it is not possible to consider the airflow stationary. Thus, according to [26], every sample must have, with respect to two previous measurements and a successive one, the following characteristics:

- u variation of less than 20%
- T variation less than 0.5° C
- SST variation less than 0.2° C
- WD changes less than 15°

The surface boundary layer height filter (in the graphs identified as "surface layer") is taken from the assumption that the PBL height z_i is proportional to u_* (with the constant ki = 0.25 and the Corioli parameter f_c, see (4.1)) and the surface layer z_s is 10% of its height (thus with ni = 0.1 see equation (4.2)) [26].

$$z_i = ki \cdot \frac{u_*}{f_c} \tag{4.1}$$

$$z_s = ni \cdot z_i \tag{4.2}$$

Nevertheless, this formulation is valid only for near-neutral conditions and this filter removes most of the very stable and very unstable conditions. z_i has to be higher than 90m in FINO-1 and 116m in Egmond aan Zee.

Since this work is aimed for offshore wind energy applications a wind speed filter is applied which selects speeds in the range 4 – 25 m/s at the hub height (i.e. cut-in and cut-out wind turbine wind speeds). This wind speed range is, in general, the operational interval of an offshore wind turbine. For Egmond aan Zee the choice of the hub height was fixed because the wind turbines, in the near offshore wind park, have 70m hub height, while for FINO-1 it has been chosen 90m hub height.

4.1 Richardson Bulk Method

The results applying MO with the definition of L using Ri_{bulk} Method are shown in Figure 4.1. The graphs are organized in the same order for all the methods, on the top of the figures there are the ones with wind speed profile (expressed as speed ratio at two elevations), in the middle the ratio of measured and predicted wind speed (u_{meas}/u_{pred}) and in the bottom the statistics of the atmospheric stratifications. The graphs are represented as a function of the non-dimensional parameter (*10/L*) in bins of 0.025. The average of the indicated value is plotted per bin.

In the top of Figure 4.1, the ratios of the wind speed between 90m and 33m for FINO-1 and 116m and 21m for Egmond aan Zee are presented. The mean value of the measurements is plotted as indication of the average wind shear for each stability bin. Associated with the mean value, the standard deviation STD of the wind shear is plotted as error bars indicating the variation per each stability condition. It is very important to know the wind speed profile for wind assessment both for aerodynamic loads and energy yield. A key-parameter for energy yield is the wind speed at hub height whereas it is relevant for load calculations (e.g. fatigue) the difference in wind speed, encountered by the rotating blade in the top and bottom positions. The model follows the measurements with a small offset for both datasets. This offset appears evident more in Egmond aan Zee than FINO-1. The filters select the data around the near-neutral conditions, excluding very stable and unstable conditions.

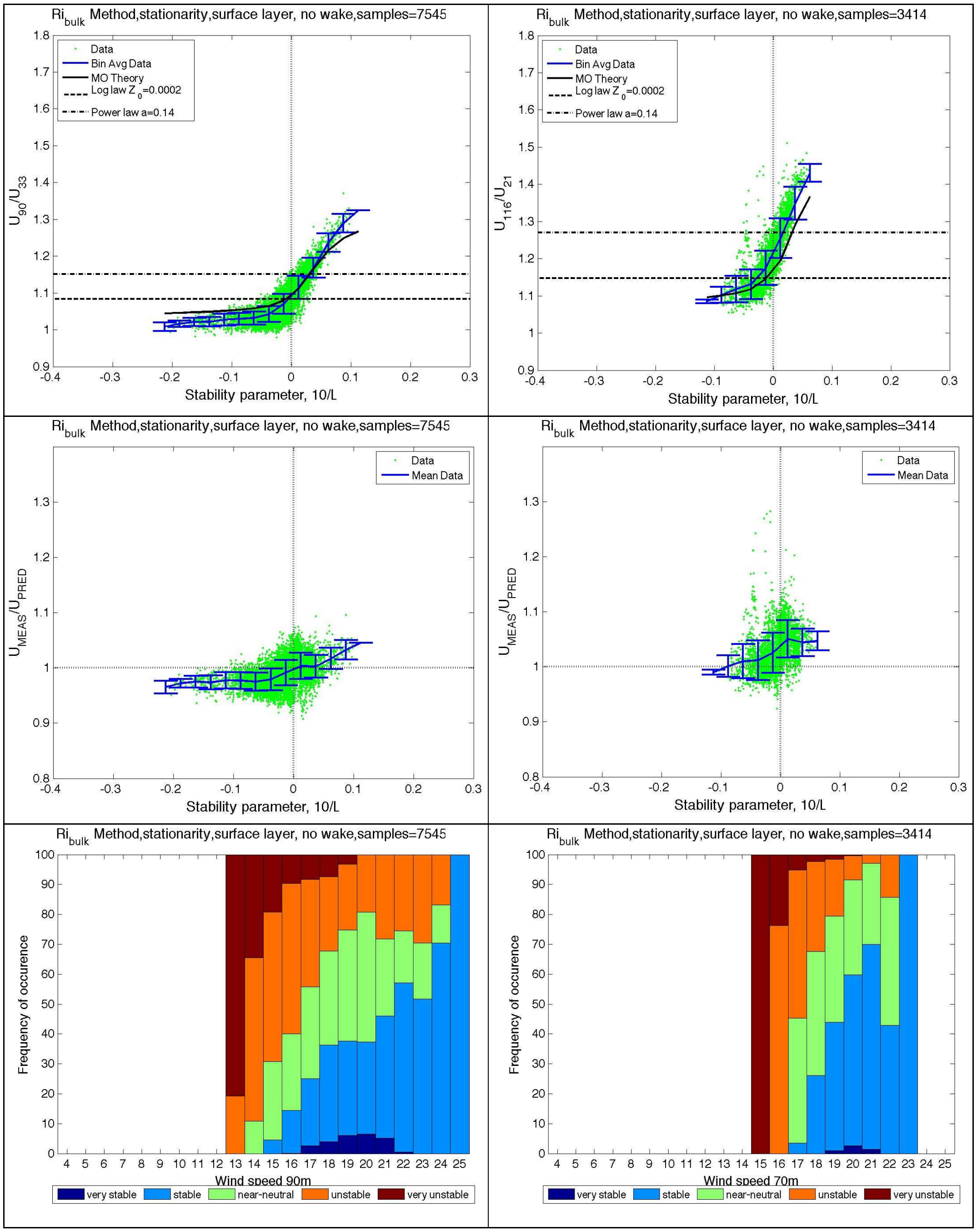

Figure 4.1: Richardson Bulk Method results for FINO-1 (left graphs) and Egmond aan Zee (right graphs). Wind speed ratio at 2 levels (top graphs), measured and predicted wind speed ratio at 90m in FINO-1 and 116m in Egmond aan Zee (middle graphs) and frequency of stratification occurrence (bottom graphs). The error bars represent the standard deviation of the data. The results are reported using stationary and surface layer filters.

In these graphs the scatter is relevant. This means that, according to Ri_{bulk} Method, the wind shear (i.e. the wind speed ratio) is not constant per stability bin. For example, for the bin 0.05 of *10/L* the ratio can be either 1.3 or 1.4 in Egmond aan Zee. So other factors influence the wind shear and/or the atmospheric stratification is not well defined by this method. Unfortunately, in Ri_{bulk} Method, the surface boundary layer filter and the stationary filter appear to be too restricting, in the sense that they exclude a lot of samples for which the surface layer is estimated to be lower than the level of the highest anemometer and the airflow is not stationary.

In the site of FINO-1 the number of samples reduces to 19% of the available data, while in Egmond aan Zee, it reduces to 5.4%. Hence, the number of data points (especially for Egmond aan Zee) is limited to make a good estimation of the wind speed profile. From the top graphs, the logarithmic equation (with $z_0 = 0.0002$) and the power law equation (with exponent $a = 0.14$) are far to fit the data. The power law always overestimates the wind shear. The log-law underestimates the wind shear in stable conditions and overestimates it in unstable ones. These considerations are quite obvious since both laws do not have stability information, but they give a general idea about the difficulties of “traditional” relations to describe the airflow in different atmospheric stratifications.

The middle graphs show the ratio of measured and predicted wind speed (u_{meas}/u_{pred}) at 90m elevation for FINO-1 and 116m for Egmond aan Zee. The graphs show the capability of the model to predict the wind speed at higher elevations knowing the wind speed below. When the values are in the neighbourhood of 1 it means that the theory works well and the assessment of the wind speed profile is well defined. When the value is less than 1 the model overestimates the wind speed and when the value is larger, the model underestimates the measurements. The model is better defined for FINO-1 than Egmond aan Zee, both for mean value and scatter.

The theory overestimates the measurements about 2% for FINO-1, considering only unstable and very unstable conditions. The overestimation decreases for near-neutral conditions in which the error reaches values of about zero. The error becomes underestimation in very stable conditions (*10/L* larger than 0.05) where it reaches about 2%.

For Egmond aan Zee, the Ri_{bulk} Method shows an underestimation that increases in near-neutral and stable conditions but it always is below 5%. The scatter is always wider than the one found in FINO-1 and it suggests that the model is not capturing all the components that influence the wind speed profile, although the average is not bad.

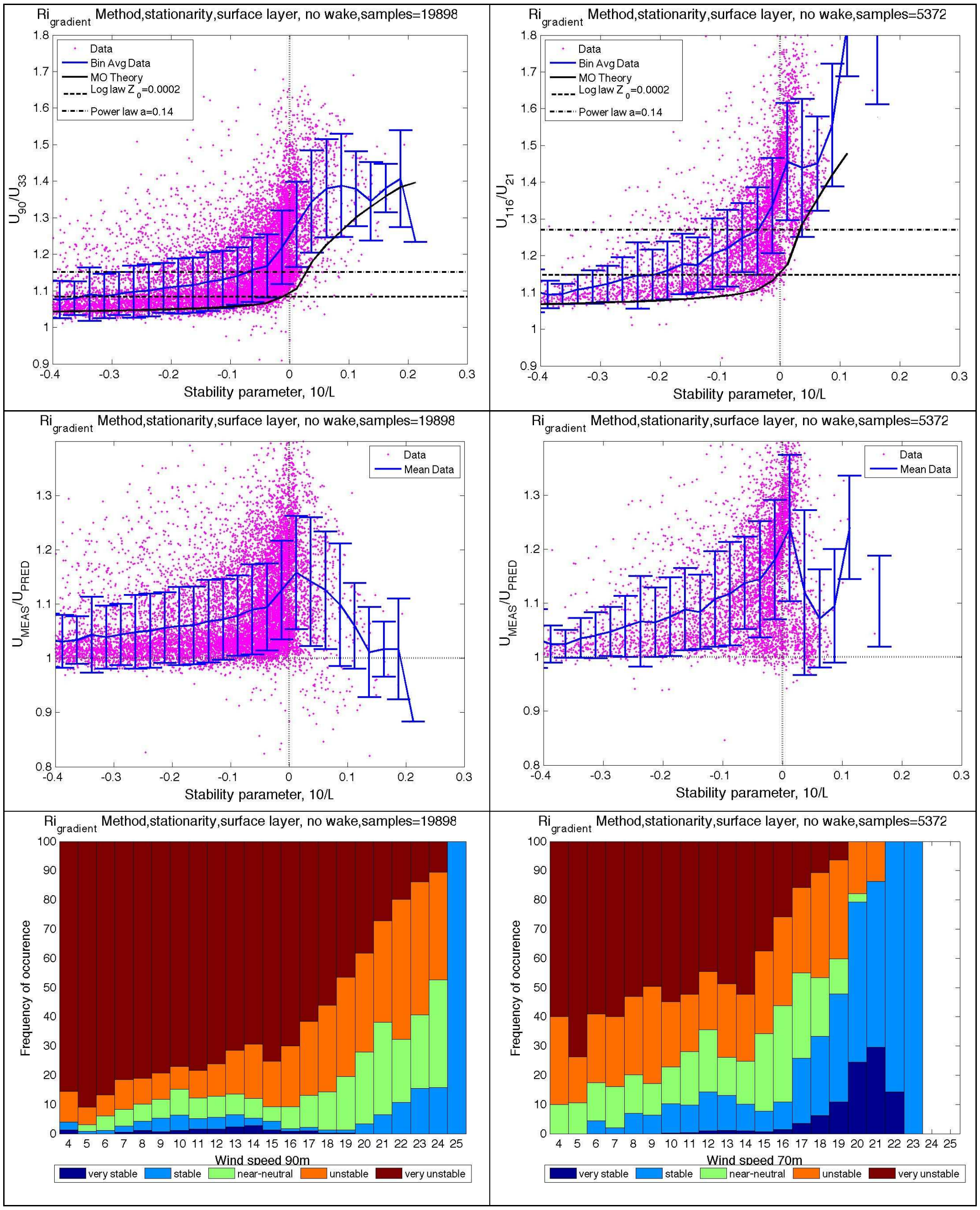

Figure 4.2: Richardson Gradient Method results for FINO-1 (left graphs) and Egmond aan Zee (right graphs). Wind speed ratio at 2 levels (top graphs), measured and predicted wind speed ratio at 90m in FINO-1 and 116m in Egmond aan Zee (middle graphs) and frequency of stratification occurrence (bottom graphs). The error bars represent the standard deviation of the data. The results are reported using stationary and surface layer filters.

In the bottom graphs of Figure 4.1 the frequency of occurrence of stability stratifications is reported as function of predicted wind speed at 90m and 70m for FINO-1 and Egmond aan Zee respectively. The importance of these graphs is easily understood in the fatigue calculation of wind turbines. It is important, for load estimations, to know how many times the wind turbine will encounter any particular wind speed profile, since the loads change with respect to different wind shear. In particular for fatigue calculations it is relevant to investigate the number of times (cycles) the wind turbine would experience the diverse wind profiles because each of them corresponds to different load amplitudes. These graphs are directly related to u_{meas}/u_{pred} because they are reliable only if the method proposed predicts the data sufficiently well. It can be noticed that the two sites seem to match in terms of stability classification. FINO-1 has less stable and more near-neutral conditions, probably due to the larger distances from the coast. The surface boundary layer filter filters more wind speeds in Egmond aan Zee than FINO-1 probably due to the fact that the reference level is 116m for the filter although the plot refers to 70m predicted wind speed. On the contrary the surface boundary layer filter in FINO-1 has the same level of the plotted results.

4.2 Richardson Gradient Method

The results of the $Ri_{gradient}$ Method are shown in Figure 4.2. In this method the wind speed difference between 33m and 50m in FINO-1 and 21m and 70m in Egmond aan Zee are used to estimate the wind speed at 90m and 116m respectively. With this method, the number of samples increases with respect to Ri_{bulk} Method. The graphs show that the data used in this model are 49.7% and 8.5% of the available data for FINO-1 and Egmond aan Zee respectively. The surface boundary layer filter is sensitive to the difference in elevation of the two wind speed measurements. For Egmond aan Zee, where this difference is large, the filter reduces the number of samples considerably compared to FINO-1. This was not the case for Ri_{bulk} Method, where the two sites had similar behaviours. Moreover the filters for the $Ri_{gradient}$ Method do not exclude the very unstable conditions.

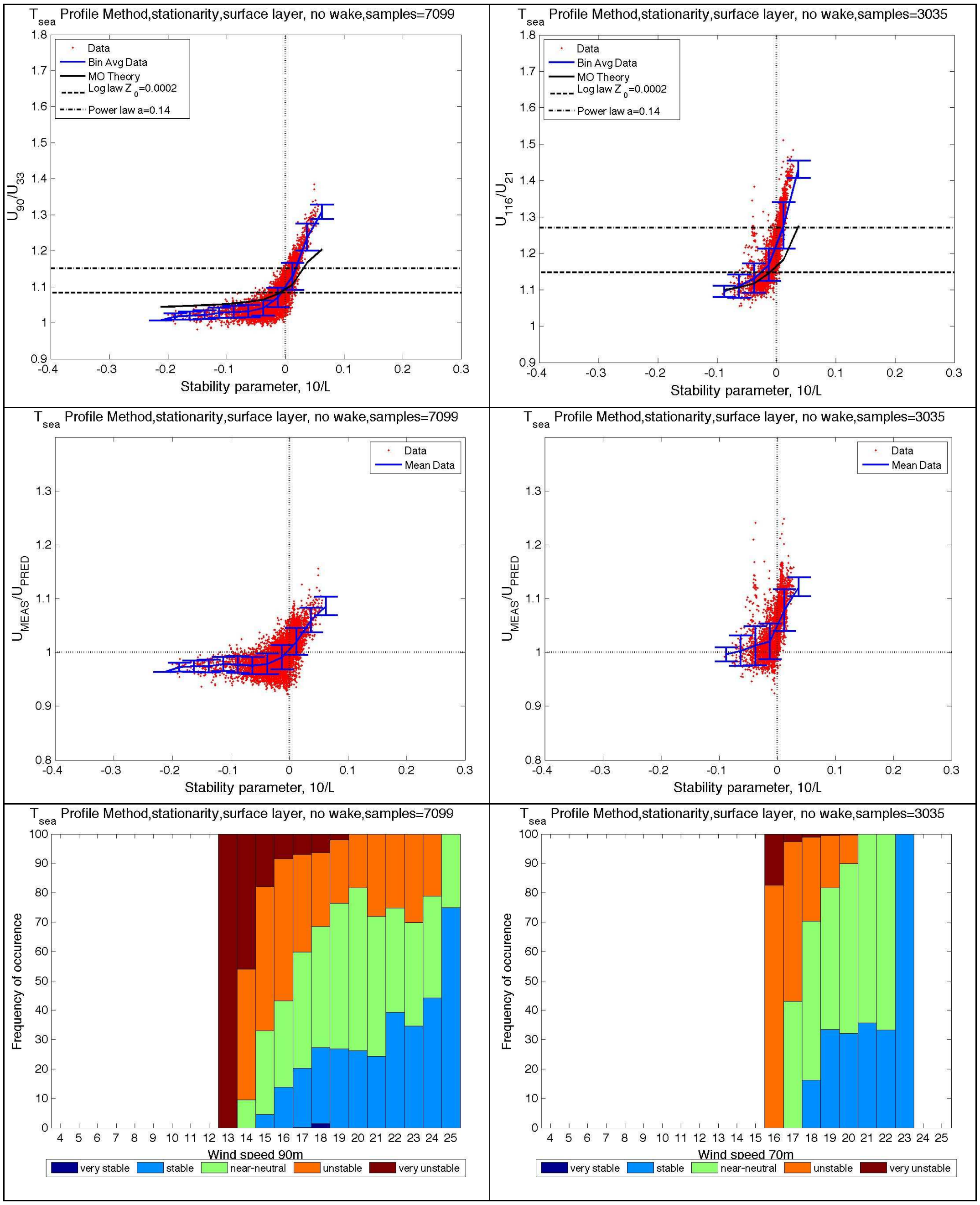

Figure 4.3: Sea Temperature Profile Method results for FINO-1 (left graphs) and Egmond aan Zee (right graphs). Wind speed ratio at 2 levels (top graphs), measured and predicted wind speed ratio at 90m in FINO-1 and 116m in Egmond aan Zee (middle graphs) and frequency of stratification occurrence (bottom graphs). The error bars represent the standard deviation of the data. The results are reported using stationary and surface layer filters.

The top graphs in Figure 4.2 show the comparison of wind shear by applying MO and measurements. The graphs seem to follow the same trend for both FINO-1 and Egmond aan Zee. The discrepancy is large in both datasets and slightly higher for Egmond aan Zee. Contrary to Ri_{bulk} Method, the model clearly underestimates the wind shear. The scatter of the measurements is relevant (around 10% of STD) and considerably higher than in the Ri_{bulk} Method. This means that the definition of stability using the $Ri_{gradient}$ Method is worse than with Ri_{bulk} Method. In the graphs the logarithmic equation (with z_0 = 0.0002) and the power law equation (with a = 0.14) are plotted as well. Again, the power law is far to fit the data in both datasets and the logarithmic law equation has good estimation only for very unstable conditions.

The graphs in the middle of Figure 4.2 show u_{meas}/u_{pred} at 90m and 116m respectively for FINO-1 and Egmond aan Zee. The model predicts the wind speed analogously for Egmond aan Zee and FINO-1. The difference between the two is evident in the number of samples that influences the solidity trend of the curve; hence in Egmond aan Zee the curve appears oscillating. Considering only very unstable conditions, the theory underestimates the measurements of about 4% in FINO-1. The underestimation increases in near-neutral and stable conditions, where it is possible to find a maximum of about 15%. In stable conditions the error decreases and, in very stable conditions there are almost no points and it is difficult to draw a conclusion. The scatter remains always high and slightly increases in stable conditions. For Egmond aan Zee the situation is similar to FINO-1, the trend is more or less the same. Here the maximum error is about 20%, for very unstable conditions it is around 3% and unstable around 10%. The scatter also increases especially in near-neutral conditions. In stable and very stable conditions, the error follows a similar trend than FINO-1, but again the number of samples influences the results.

The frequency of occurrence of stratifications is reported as a function of predicted wind speed. The two sites differ in terms of stability classification. FINO-1 has greater number of unstable conditions, with practically no stable conditions, while Egmond aan Zee shows higher stable stratifications for large wind speeds. The stability classification is slightly different from the Ri_{bulk} Method but here stable and near-neutral conditions increase with high wind speeds. This behaviour is evident in the Ri_{bulk} Method too, but the low wind speeds are not present.

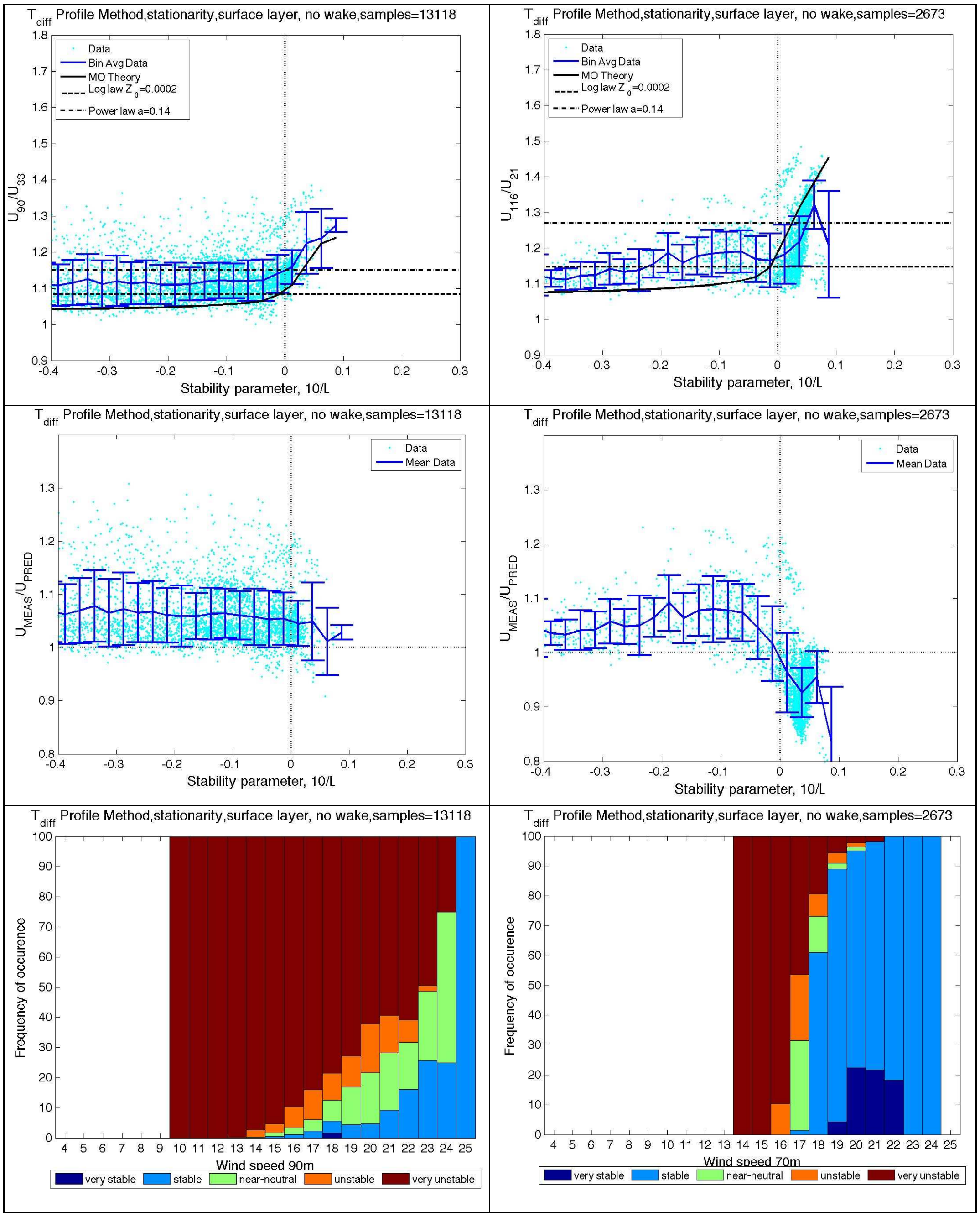

Figure 4.4: Temperature Difference Profile Method results for FINO-1 (left graphs) and Egmond aan Zee (right graphs). Wind speed ratio at 2 levels (top graphs), measured and predicted wind speed ratio at 90m in FINO-1 and 116m in Egmond aan Zee (middle graphs) and frequency of stratification occurrence (bottom graphs). The error bars represent the standard deviation of the data. The results are reported using stationary and surface layer filters.

4.3 Sea Temperature Profile Method

The first results of the profile methods are from T_{sea} Profile Method and are shown in Figure 4.3. The measurements used are u, T and RH at 33m and T_m at - 3m (that is assumed to be the *SST*) for the dataset of FINO-1. The same measurements are taken for Egmond aan Zee but at different levels, 21m and -3.8m respectively. The results are similar to Ri_{bulk} Method and this behaviour is reasonable (according to [14]) because when the profile method uses all the measurements of u, T and RH at the same level with accurate substitution, the Ri_{bulk} relations can be derived. T_{sea} Profile Method agrees with the Ri_{bulk} Method better in FINO-1 than Egmond aan Zee. Indeed, for Egmond aan Zee, a lager offset can be observed between the model and the data. The scatter resembles the Ri_{bulk} Method and the considerations made are the same here. The number of samples resembles also the Ri_{bulk} Method and indeed for FINO-1 it is 17.7% of the available data and for Egmond aan Zee 4.8%.

For the middle graphs, the consideration made previously for the Ri_{bulk} Method are valid for FINO-1, while of Egmond aan Zee the model shows a slightly higher underestimation in stable conditions.

The statistics of atmospheric stratifications show a similar behaviour with respect to Ri_{bulk} Method, but here for both sites a higher concentration can be noticed of near-neutral stratifications.

4.4 Temperature Difference Profile Method

The following results are from the T_{diff} Profile Method and are shown in Figure 4.4. The measurements used in this method are u at one level and T and the respective RH at two levels. u is taken at 33m and T at 33m and 50m above the m.s.l. for the dataset of FINO-1. At Egmond aan Zee u is taken at 21m and T and RH at 21m and 70m. The number of samples is similar to $Ri_{gradient}$ Method and indeed for FINO-1 it is 32.7% of the available data and 4.2% for Egmond aan Zee. As observed for $Ri_{gradient}$ Method the higher distance of the anemometers in Egmond aan Zee produces a stricter surface boundary layer filter.

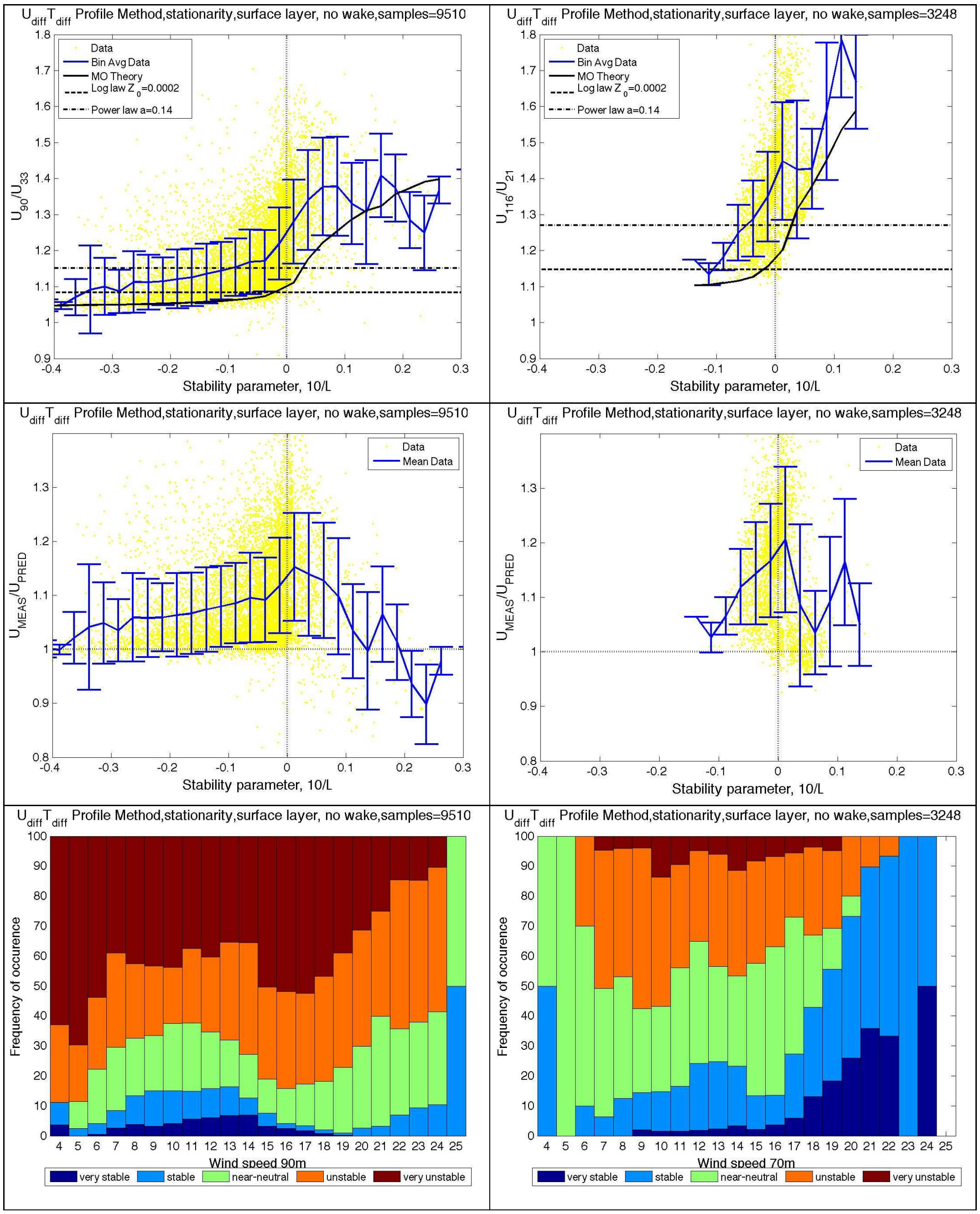

Figure 4.5: Wind Speed and Temperature Difference Profile Method results for FINO-1 (left graphs) and Egmond aan Zee (right graphs). Wind speed ratio at 2 levels (top graphs), measured and predicted wind speed ratio at 90m in FINO-1 and 116m in Egmond aan Zee (middle graphs) and frequency of stratification occurrence (bottom graphs). The error bars represent the standard deviation of the data. The results are reported using stationary and surface layer filters.

The graphs of Figure 4.4 show the wind shear from measurements and theory. In this method, the model fits better the measurements, if compared to $Ri_{gradient}$ Method, but worse compared to T_{sea} Profile Method or Ri_{bulk} Method. With T_{diff} Profile Method the logarithmic law defines accurately the wind shear in the two sites for very unstable, unstable and near neutral conditions. In stable conditions, however, the model does not predict the wind shear well. The power law is not very accurate and always overestimates the wind shear. The ratio u_{meas}/u_{pred} is more or less constant for all stratifications in FINO-1 and equals to 5% of the underestimated values. u_{meas}/u_{pred} oscillates around 5% for Egmond aan Zee and decreases suddenly for near-neutral conditions to almost zero and in stable ones reaches more than 5 % of the overestimated values. The scattering is relevant for both sites and greater than T_{sea} Profile Method.

The graphs of the atmospheric stratifications show that the two sites are different from an atmospheric stratification distribution point of view. More than 70% of the stratifications are in the very unstable region for FINO-1 while for Egmond aan Zee the largest part is in the stable conditions. Surprisingly, such difference between the two sites is not present in any of the previous methods and also almost the absence of the near-neutral class is sign that the model is not working correctly

.

4.5 Wind Speed and Temperature Difference Profile Method

The results from $U_{diff}T_{diff}$ Profile Method are shown in Figure 4.5. The wind speed difference between two levels and the air temperature difference between other two levels (that in general can be different) are used. The measurements considered are *u*, *T* and *RH* at 33m and 50m for FINO-1. For Egmond aan Zee these levels are 21m and 70m. The number of samples is 23.7% and 5.1% of the available data respectively for FINO-1 and Egmond aan Zee. The results show a similar trend to the one of the $Ri_{gradient}$ Method, only in Egmond aan Zee the profile method cuts off the very unstable conditions.

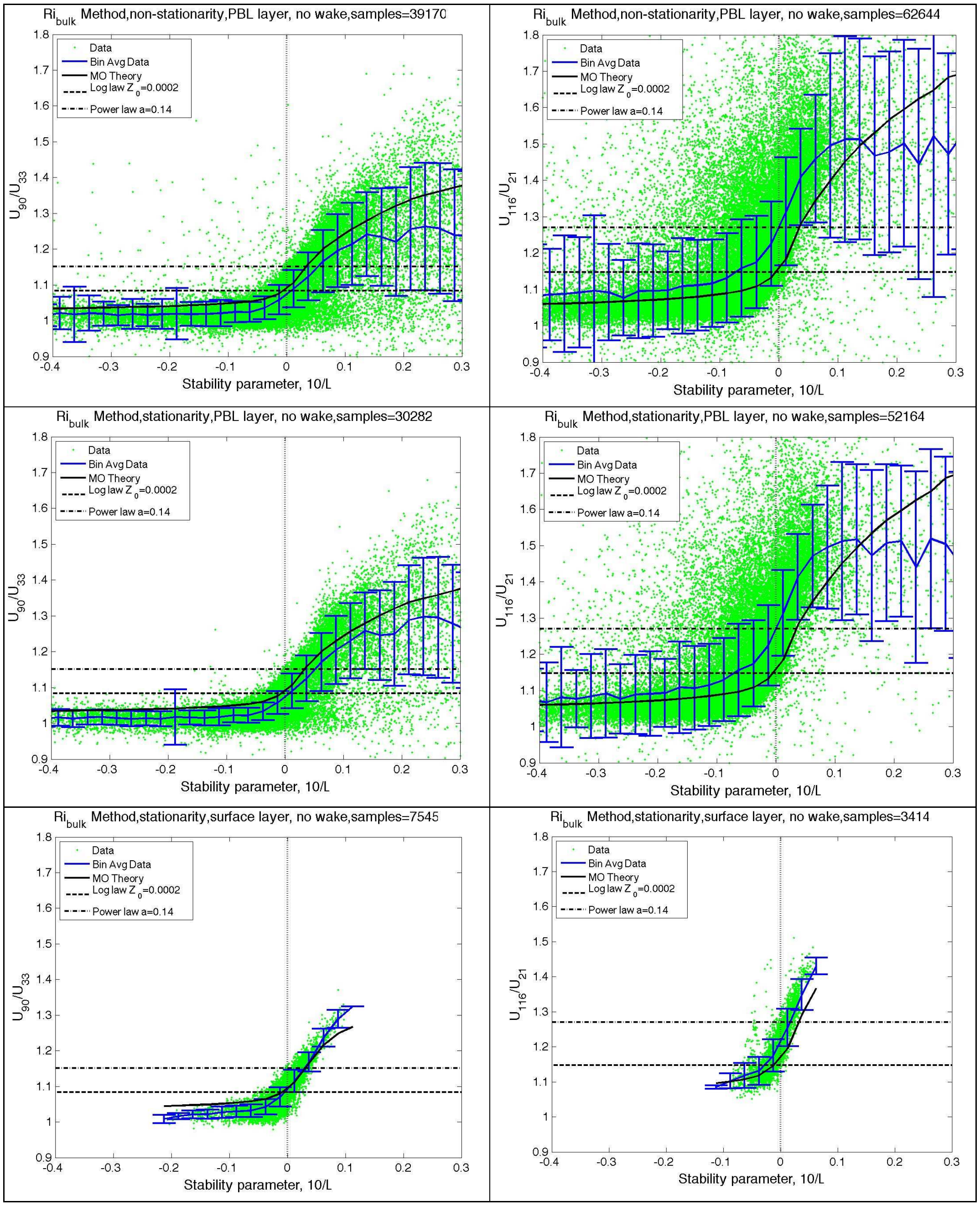

Figure 4.6: Wind speed ratio at 2 levels without filters (top graphs), with stationary filter (middle graphs) and with both stationary and surface layer filters (bottom graphs) using the Richardson Bulk Method. The error bars represent the standard deviation of the data. On the left side the data from FINO-1 and on the right side Egmond aan Zee.

The top graphs in Figure 4.5 show the wind shear ratio between 33m and 90m in FINO-1 and 21m and 116m in Egmond aan Zee. The model fits the data in the same way both in Egmond aan Zee and FINO-1. There is in both graphs an offset between the model and the bin average data. The model estimates always a lower wind shear than the measurements except in very stable conditions where the offset between model and measurements decreases. However in very stable conditions the number of samples is actually small to draw conclusions. The scattering is considerably high in both sites, especially in stable and very stable conditions. The wind speed estimated with this model is really poor especially for Egmond aan Zee, where in near-neutral conditions the error reaches 20% of the underestimated values. For FINO-1 there is a constant underestimation offset that increases slightly in neutral conditions and decreases for stable ones.

The two sites appear completely different from stratification distribution point of view, as already noticeable in the T_{diff} Profile Method. Egmond aan Zee almost misses very unstable conditions while in FINO-1 they are the majority. Moreover, stable and very stable conditions are less than 10% in FINO-1 for almost all wind speeds. In Egmond aan Zee stable and very stable conditions are present only for high wind speeds.

4.6 Stationarity and Surface Layer Height

The models presented show different behaviours in predicting the wind speed profile. This is due to the different assumptions and manners to estimate L. The best model is Ri_{bulk} Method for both FINO-1 and Egmond aan Zee. This model shows results similar to T_{sea} Profile Method because Ri_{bulk} Method is a simplification of this model and a direct measure of the atmospheric stability [14]. The model shows errors in estimating the wind speed and the scatter is not negligible in both sites. Even the average is not correct, especially for Egmond aan Zee where the model reports a general underestimation of the wind shear. In stable and very stable conditions both sites show underestimation as already reported in [8]. Indeed stable conditions are, for all the models, the critical ones. Hence, Ri_{bulk} Method is selected as reference model to estimate L and it is used for the further analyses.

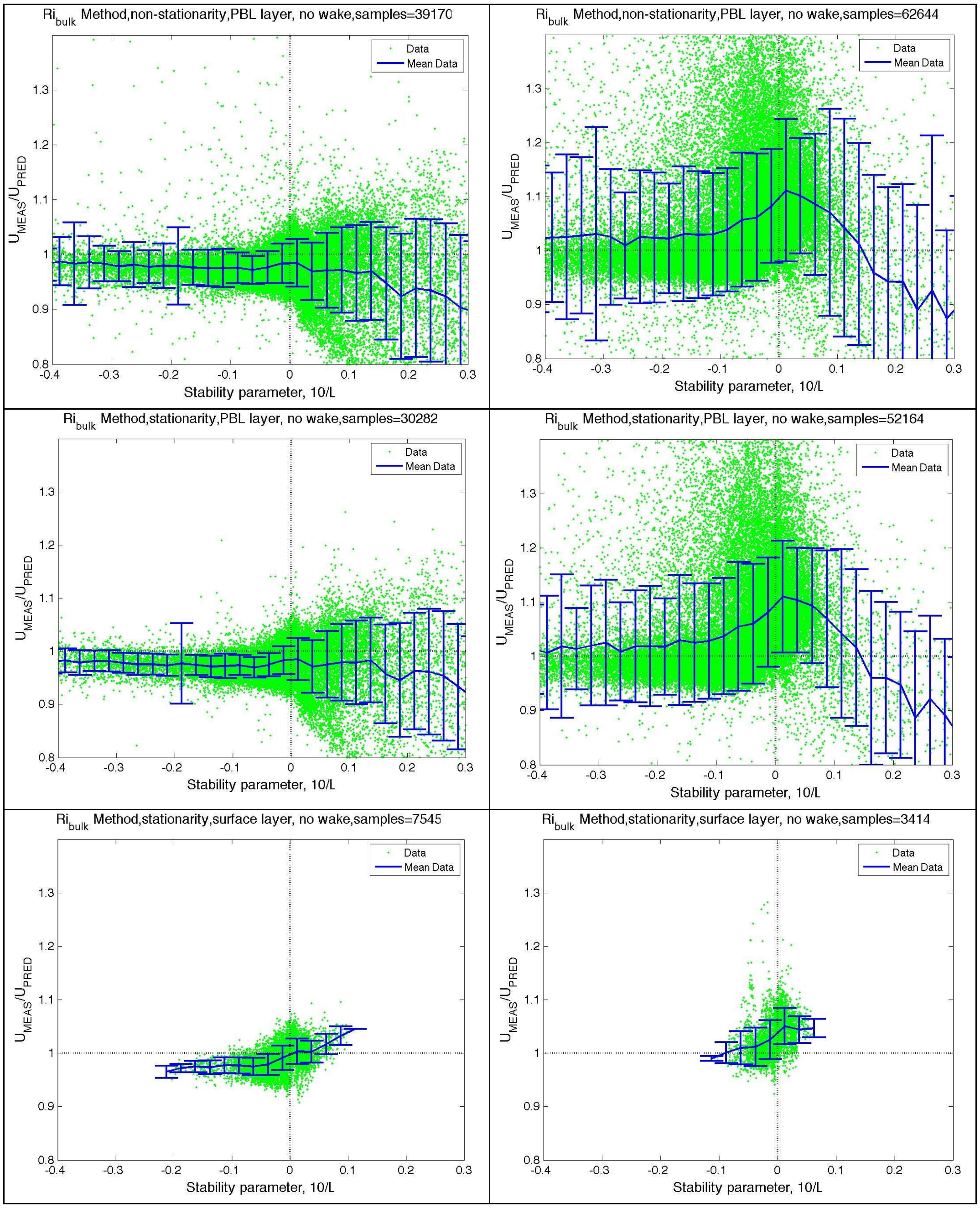

Figure 4.7: Measured and predicted wind speed ratio at 90m in FINO-1 and 116m in Egmond aan Zee without filters (top graphs), with stationary filter (middle graphs) and with both stationary and surface layer filters (bottom graphs) using the Richardson Bulk Method. The error bars represent the standard deviation of the data. On the left side the data from FINO-1 and on the right side Egmond aan Zee.

The MO Similarity Theory is founded on the assumptions of stationary and constant u_* within the layer of interest, i.e. the highest level of the considered anemometer. For these reasons two filters are applied to the measurements. In this part of the work the effects of these assumptions on the results are shown for Ri_{bulk} Method in Figure 4.6, Figure 4.7 and Figure 4.8. The graphs on the top of each figure illustrate the results with non-filtered data, the graphs in the middle with only the stationary filter and the graphs in the bottom with both filters.

The first observation that can be made is the reducing number of samples by applying the different filters. However, even when no filters are applied, the Ri_{bulk} Method reduces the number of available data (because the model is not valid for Ri_b larger than 0.2, see theory in section 2.1). Hence the numbers of available data are 98% and 99.7% of the original measurements respectively for FINO-1 and Egmond aan Zee, when no filter is applied. However, this reduction is not relevant. Instead, when the stationary filter is applied, the number of 10-min samples shrinks by 22.7% of the available data for FINO-1, while for Egmond aan Zee it drops only by 16.8%. When the surface boundary layer is applied to the stationary condition measurements, it shrinks the samples by 75% and 93.5% for FINO-1 and Egmond aan Zee respectively.

Figure 4.6 shows the trend of the wind shear with respect to the stability. The model follows the mean value of the data with an offset for both sites and almost no difference can be noticed between non-filtered and stationary conditions. Only in the unstable part a reduction in the scatter can be noticed in FINO-1 and a slight reduction in Egmond aan Zee for all stratifications. The situation changes in the bottom graphs where the offset decreases, if compared to the same range of stability (*10/L*) in the previous graphs. Here a small underestimation offset remains in Egmond aan Zee while in FINO-1 a perfect match exists in near-neutral conditions, an underestimation in stable conditions and an overestimation in the unstable part.

Figure 4.7 shows the effect of the filters in the wind speed prediction at 90m and 116m. The first observation that can be made is the progressive reduction of the scatter (the STD) when the filters are applied. This was expected since the model is based on certain assumptions that are fulfilled via the filters. Nevertheless, the scatter is still relevant and this means that other factors influence the offshore wind shear. The average remains slightly the same when the stationarity is applied but it changes when the surface boundary layer filter is considered. With only the stationary filter the behaviour of the model is different in predicting the wind speed profile.

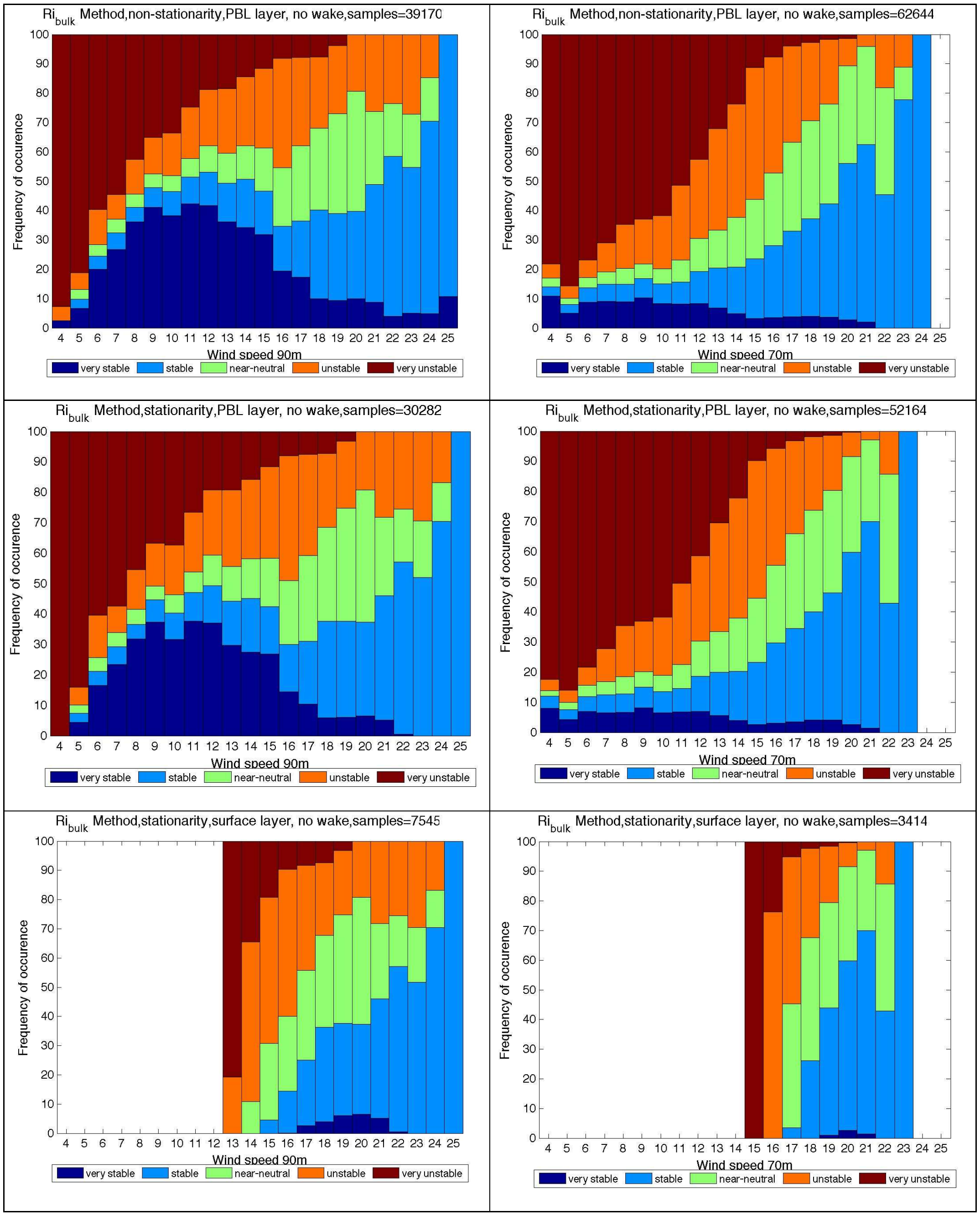

Figure 4.8: Frequency of occurrence of atmospheric stratifications without filters (top graphs), with stationary filter (middle graphs) and with both stationary and surface layer filters (bottom graphs) using the Richardson Bulk Method. The error bars represent the standard deviation of the data. On the left side the data from FINO-1 and on the right side Egmond aan Zee.

A general overestimation can be noticed for all stratifications for FINO-1, while there is a considerable increase in underestimation for near-neutral and stable conditions in Egmond aan Zee. With the two filters, the prediction is better but the number of samples indicates that this prediction is valid for a small amount of time. In other words, it is not really possible to estimate the wind profile for all conditions using MO.

Figure 4.8 shows the frequency of occurrence of atmospheric stratifications when the different filters are applied with respect to the predicted wind speed at 90m and 70m. The presence of the stationary filter does not alter the frequency of occurrence. The graphs, both for FINO-1 and Egmond aan Zee, appear to be similar. This means that statistically, any atmospheric stratification (very stable, very unstable, etc.) for any wind speed bin has the same amount of non-stationary conditions. When the surface layer is applied, the graphs change. The low wind speeds are deleted but for high wind speeds the percentage of the stratifications remains more or less the same. The surface layer filter eliminates thus the low wind speeds where u_* cannot be considered constant, maintaining the same samples for high wind speeds.

Chapter 5

SENSITIVITY OF THE INPUT PARAMETERS

In this chapter, the effects of the input parameters on Ri_{bulk} Method are investigated. To this aim the chapter is divided in few parts. The MO theory is based on many assumptions and different parameters are necessary to estimate the wind profile. In literature, different definitions are given for variables like T, SST, RH, Charnock's coefficient, PBL height and surface boundary layer height. Further the effects of distance from the coast and reference u are treated.

5.1 Effect of Temperature

Temperature is a key-factor in the definition of L, although often it is not clear which kind of temperature is required (or better saying suitable) to define Ri_b. In this paragraph combinations of temperatures are proposed as input for Ri_{bulk} Method and their effects are reported as function of u_{meas}/u_{pred} for the aforementioned offshore databases. As explained in theory, Ri_b (see equation (2.18)) needs the temperature at the lower boundary condition, i.e. the air temperature at the interface between seawater and air (in this work called $T_{air\text{-}sea}$, see Figure 2.1), and T at one level. The $T_{air\text{-}sea}$ used in the model can be either the T_{sea} or Tv_{sea}. For the air temperature four conditions can be assumed: T, T_v, θ and θ_v.

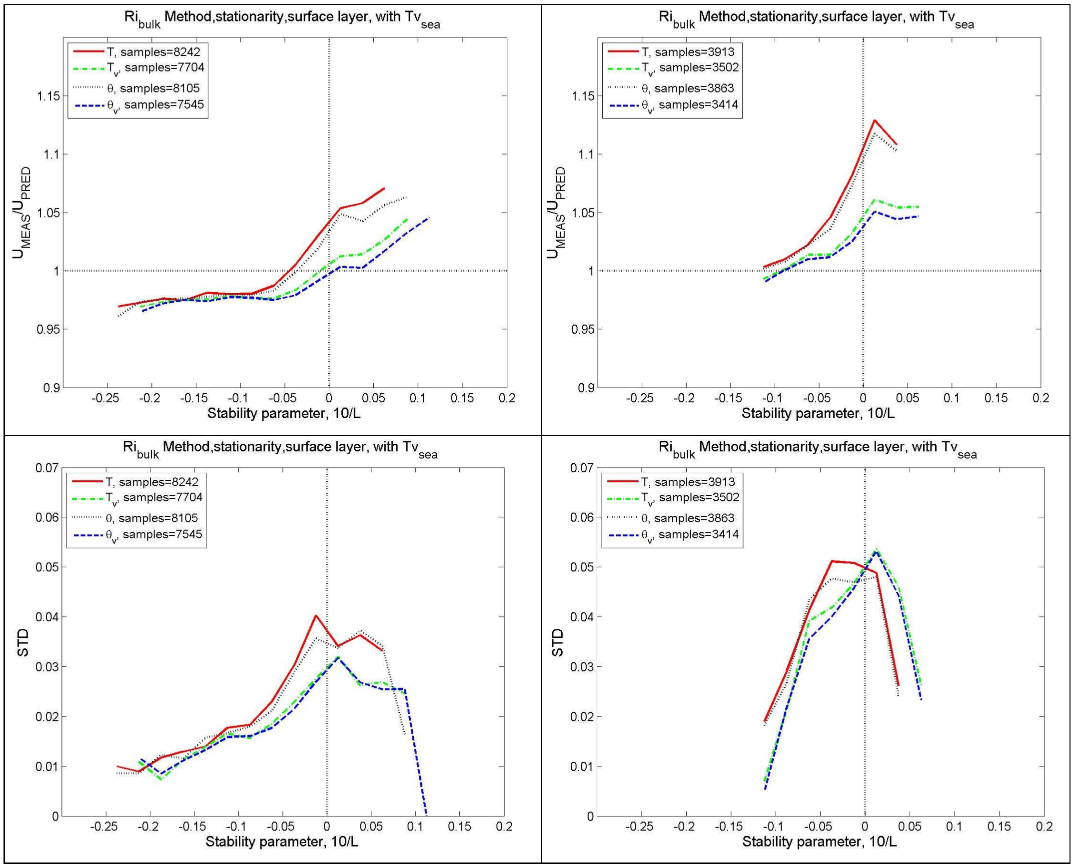

Figure 5.1: Air temperature definition influence on predicted wind speed at 90m in FINO-1 and 116m in Egmond aan Zee using Richardson Bulk Method. The results are shown in terms of average measured and predicted wind speed ratio (top graphs) and its standard deviation (bottom graphs) for 4 temperatures (absolute T, virtual T_v, potential θ and virtual potential θ_v). The virtual sea surface temperature Tv_{sea} is used as reference. Both the stationary and the surface layer filters have been applied. On the left side the data from FINO-1 and on the right side Egmond aan Zee.

Figure 5.1 and Figure 5.2 show the effects of temperature in terms of bin averaged u_{meas}/u_{pred} and the standard deviation of u_{meas}/u_{pred}. In Figure 5.1 the results are plotted using Tv_{sea} (that was utilised so far for all the analyses) and the four air temperatures, while in Figure 5.2 the two sea surface temperature are compared using θ_v as reference air temperature. Considerable changes in the ratio u_{meas}/u_{pred} can be noticed in Figure 5.1 when different air temperatures are considered and especially when the virtual condition is applied (i.e. when the RH is considered). The effects of the pressure are not evident from the results, indeed T and θ follow the same trend. When the RH is applied, u_{pred} is higher than with T and θ and hence u_{meas}/u_{pred} is closer to 1. The STD as well expresses this change in u_{pred} in particular for FINO-1, where in near-neutral and stable conditions the STD reduces of about 1%. Instead in Egmond aan Zee the STD does not change considerably.

From Figure 5.1 it can be concluded that θ_v is the best choice as air temperature for the Ri_b Method. Thus, using θ_v as reference, in Figure 5.2 the comparison between T_{sea} and Tv_{sea} is presented. The effect of changing $T_{air\text{-}sea}$ is evident especially for near-neutral and stable stratifications. For both databases the use of T_{sea} increases (on average) u_{pred} and hence the model overestimates the wind shear (u_{meas}/u_{pred} less than 1). This behaviour was expected since using T_{sea}, instead of Tv_{sea}, means reducing the value of $T_{air\text{-}sea}$ in all stratifications. However, in near-neutral and stable conditions, this smaller $T_{air\text{-}sea}$ value creates a smaller temperature difference and hence the airflow is considered less stable. This means that with a smaller temperature difference the model predicts (on average) a smaller wind shear and this is evident in the graphs around the near-neutral stratification (-0.05 < *10/L* < 0.05). The STD does not give particular information using Tv_{sea} or T_{sea}.

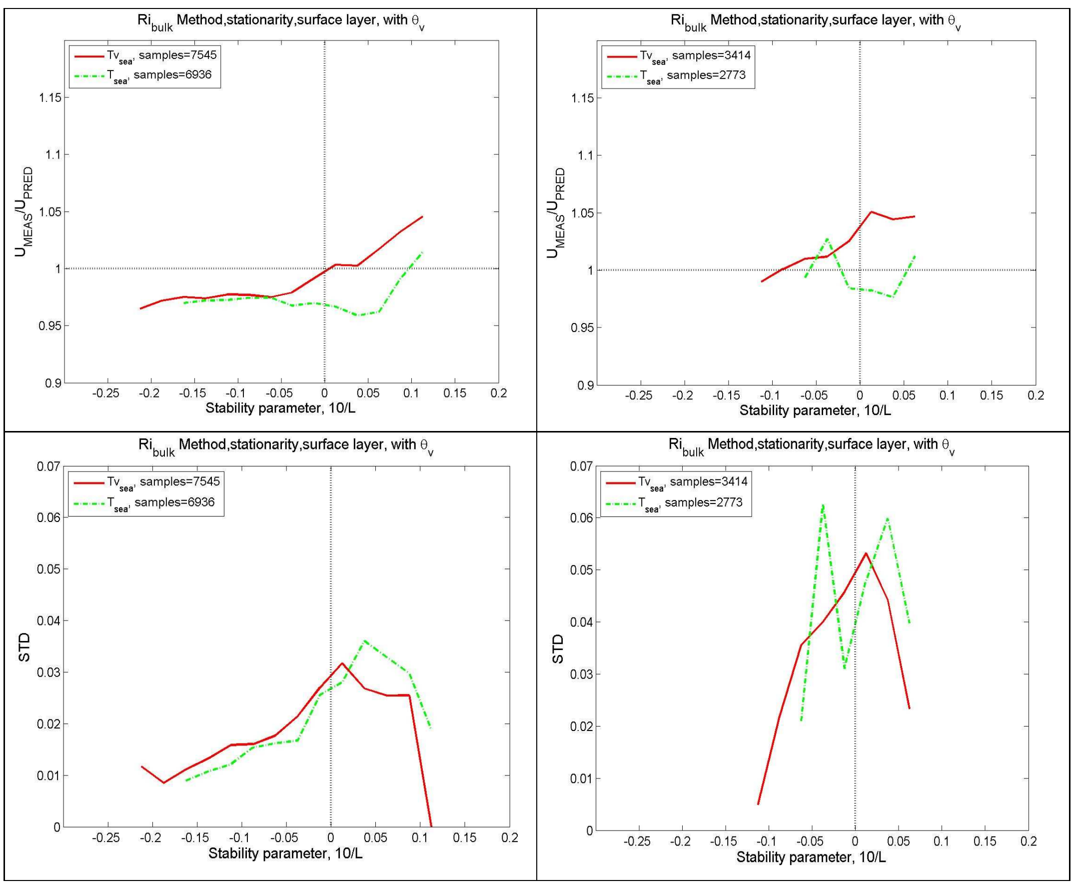

Figure 5.2 Virtual (Tv_{sea}) and absolute (T_{sea}) sea surface temperature influence on predicted wind speed at 90m in FINO-1 and 116m in Egmond aan Zee using Richardson Bulk Method. The results are shown in terms of average measured and predicted wind speed ratio (top graphs) and its standard deviation (bottom graphs) with virtual potential θ_v as air temperature reference. Both the stationary and the surface layer filters have been applied. On the left side the data from FINO-1 and on the right side Egmond aan Zee.

The number of samples is influenced by the choice of the temperature too. In the legend of Figure 5.1 the number of samples is indicated accordingly to the air temperature. This means that the temperature choice influences also the definition of the atmospheric boundary layer and, as consequence, the surface boundary layer height and hence the effectiveness of the surface layer filter. The largest number of samples (both for FINO-1 and Egmond aan Zee) is found using T, while the smallest is with θ_v. This behaviour can be explained considering how the surface boundary layer filter is defined. z_s is directly proportional to u_*, which is calculated rearranging (2.9), i.e. equation (2.25) explained in section 2.3.1, in order to get u_* as a function of u. From this equation, it can be noticed that u_* is inversely proportional to the stability function Ψ_m, which, in this case, is linked to Ri_b. The Ri_b is directly proportional to the temperature difference between sea and air, bigger the difference larger the Ri_b. In stable conditions, when Ri_b is large, u_* is small (assuming of course same u) and vice versa when Ri_b is small u_* is large. Hence using T (when the air is warmer than the sea) the temperature difference is lower and z_s is higher, thus the number of samples is larger. Vice versa using θ_v the difference is higher and z_s is low, consequently the number of samples decreases. In unstable conditions u is on average smaller (see also Figure 5.10 in section 5.3) and so the effect of Ψ_m in the denominator of equation (2.25) is not relevant to determine whether the filter applies or not. Analogously (referring to Figure 5.2), the samples using Tv_{sea} are larger than with T_{sea}, since in stable conditions the difference is smaller because the value of $T_{air\text{-}sea}$ becomes higher when RH is taken into account. From the results of Figure 5.1 and Figure 5.2 and for sake of consistency the chosen combination of temperatures, for the following analyses, is Tv_{sea} and θ_v.

5.2 Effect of Surface Layer Height

The surface boundary layer is the most severe filter of the two, since it reduces drastically the number of measurements in both databases. The filter is related to the definition of the *PBL* height and to z_s height. As suggested in literature (see for example [26]), the coefficient (called in this work for simplicity *ki*) that relates the *PBL* height to the u_* in relation (4.1) is equal to 0.25 and the coefficient (called here *ni*) that defines z_s is 0.1. Since these coefficients are not accurate, the wind speed profile estimation is analysed using different *ki* and *ni*.

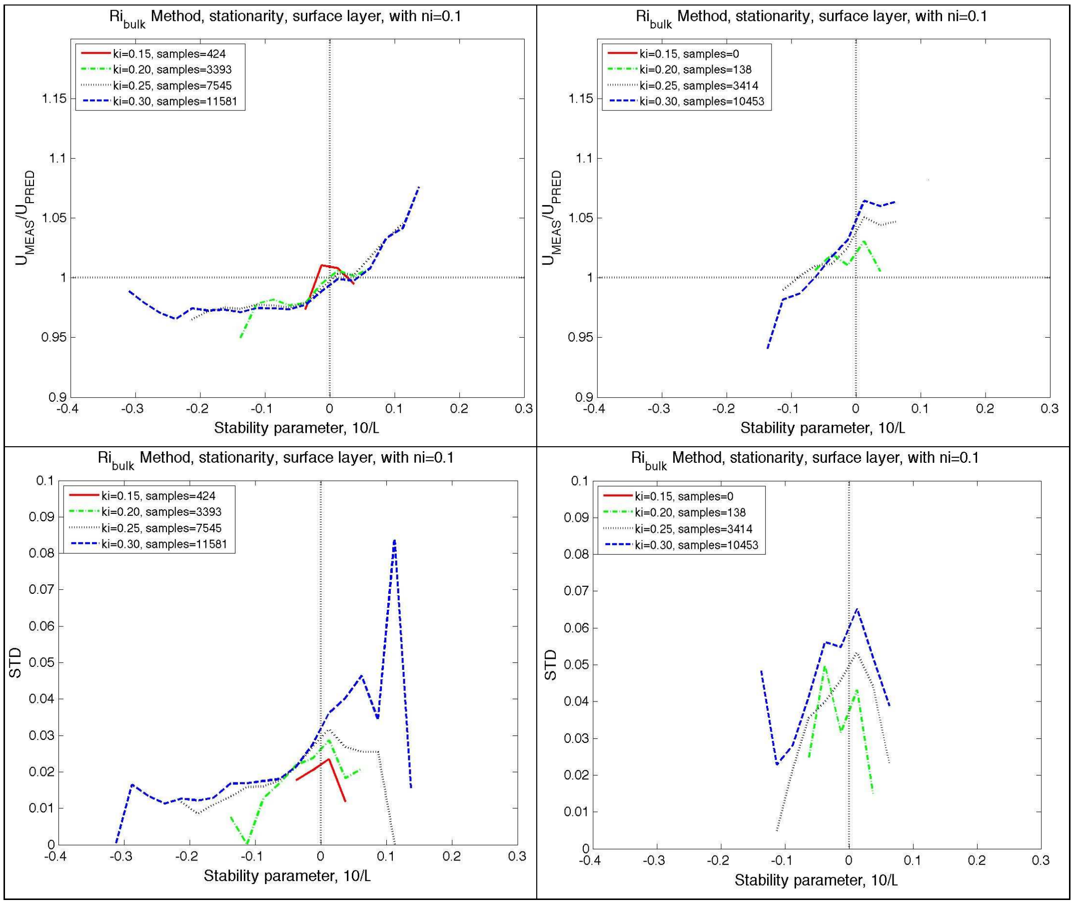

Figure 5.3 Atmospheric boundary layer (PBL) height influence on predicted wind speed at 90m in FINO-1 and 116m in Egmond aan Zee using Richardson Bulk Method. The results are shown in terms of average ratio of measured and predicted wind speed (top graphs) and standard deviation (bottom graphs) for 4 values of *ki*. The virtual sea surface temperature Tv_{sea} is used as reference. On the left side the data from FINO-1 and on the right side Egmond aan Zee.

Figure 5.3 shows the effects of changing *ki* with constant *ni* for the two offshore sites. The values range from 0.15 to 0.30. The two sites show different behaviour. In FINO-1 the average maintains the same trend with changing *ki*, while STD increases considerably in very stable conditions (as well the mean error), especially when a higher value of *ki* is used. The behaviour is different for Egmond aan Zee and the average error increases accordingly to *ki*. The same can be said for the STD, but here it is less evident than in FINO-1. The number of samples increases with increase *ki* and this is obvious since for the same conditions of u_* the PBL is larger; hence z_s height is higher than the considered anemometer elevation. What is relevant is that the rate of increasing number of samples is actually different between the two sites. For Egmond aan Zee the rate is extremely high while for FINO-1 is lower. When *ki* decreases, the number of samples decreases, but the results improve only in the mean wind speed prediction for Egmond aan Zee.

Both the sites maintain large STD when *ki* = 0.20, which is similar to the original condition. When *ki* is 0.15 the number of sample reaches value of zero in Egmond aan Zee and 424 in FINO-1, hence this value cannot be taken into account.

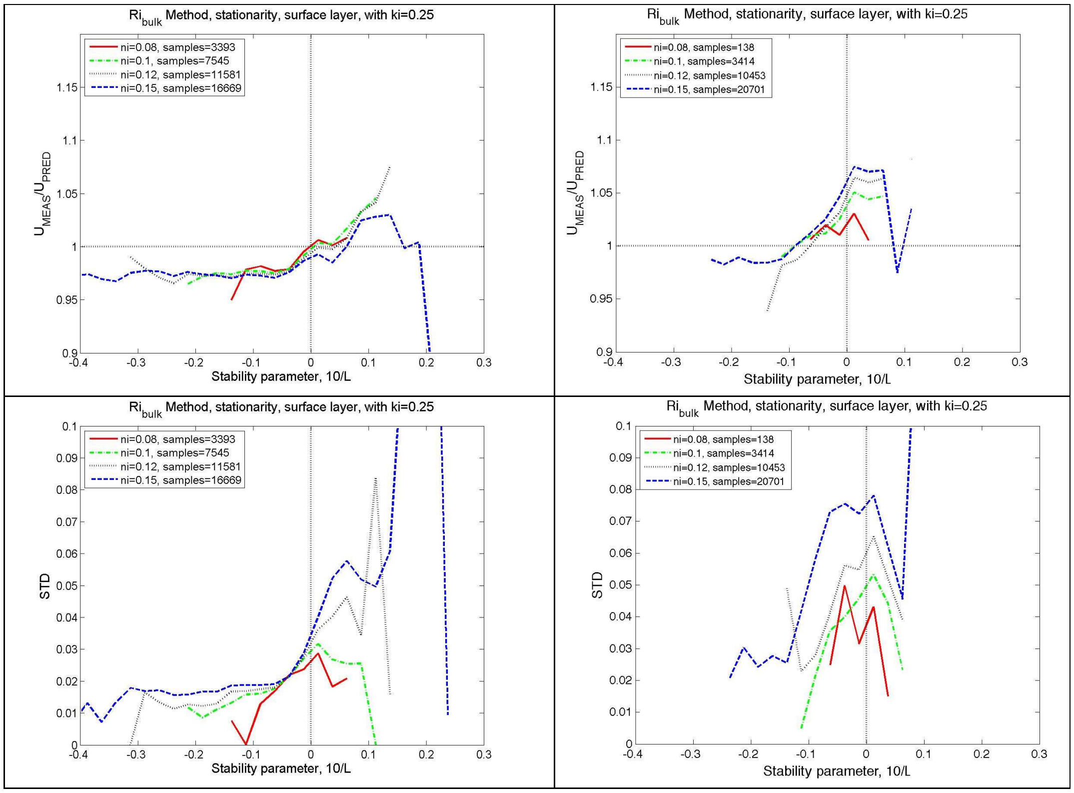

Figure 5.4: Surface layer height influence on predicted wind speed at 90m in FINO-1 and 116m in Egmond aan Zee using Richardson Bulk Method. The results are shown in terms of average ratio of measured and predicted wind speed (top graphs) and standard deviation (bottom graphs) for 4 values of *ni*. The virtual sea surface temperature Tv_{sea} is used as reference. On the left side the data from FINO-1 and on the right side Egmond aan Zee.

Figure 5.4 is similar to the previous picture and it shows the effects of changing *ni* with constant *ki*. The effects are similar to those seen in Figure 5.3 and it is quite reasonable since it is a matter of multiplying constants. What is interesting is that for *ni* = 0.15 the number of samples is considerably high (more than 30% for both sites) and the average of wind speed estimation is actually reasonable for very stable conditions, but the standard deviation is out of range. This fact underlines how the model lacks accuracy and is ineffective when high stable stratifications are considered. Indeed the mean and STD are reasonably good for very unstable, unstable, near-neutral and stable conditions, but for very stable conditions a peak of 20% STD is encountered for FINO-1 and 10% for Egmond aan Zee. Decreasing z_s height, the mean value is almost stable in FINO-1 and the standard deviation slightly decreased; on the other hand

Egmond aan Zee shows better mean wind speed estimation but not a considerably decrease in STD. The decrease in number of samples is relevant and too few data points are available to ensure reliable results.

As previously stated, the definition of z_s is only valid in near-neutral conditions because it is related directly to the height of PBL. According to [5], PBL height is function of L. For near-neutral and stable conditions, it can be assumed that it is proportional to the surface fluxes. When the airflow is unstable the determination of the height is complicated because it depends on the history of the surface heat flux and on the lapse rate above the boundary layer. Good estimation of *PBL* height can be obtained, in unstable conditions, only with direct measurements. For meteorological applications, equations (5.1) are suggested [5]. Equations (5.2) are indicated for obtaining a smoother transition between stable and neutral conditions.

$$
\begin{aligned}
z_i &= 0.3 \cdot (u_* / f_c), near-neutral \\
z_i &= 0.4 \cdot (u_* / f_c L)^{1/2}, stable \\
z_i &= 0.3 \cdot (u_* / f_c), unstable
\end{aligned}
\tag{5.1}
$$

$$
\begin{aligned}
z_i / L &= \frac{\left[1 + 2.28 \cdot (u_* / f_c L)\right]^{1/2}}{3.8}, near-neutral \\
z_i / L &= \frac{\left[1 + 2.28 \cdot (u_* / f_c L)\right]^{1/2}}{3.8}, stable \\
z_i &= 0.3 \cdot (u_* / f_c), unstable
\end{aligned}
\tag{5.2}
$$

The effects of using different equations for *PBL* are shown in Figure 5.5. The results are shown for the two equations and for the original equation used so far to define z_s height (see equation (4.1)). (Note: in the graphs for simplicity equations (5.1) are called van Wijk v.1 and equations (5.2) van Wijk v.2, since A.J.M. van Wijk is the first author of [5]). The graphs show that the two formulas of van Wijk are similar. Only the number of samples decreases applying equations (5.2). Anyway these new equations appear to be extremely severe for stable conditions where in both databases no points are present. In the other conditions the original equations (4.1) seem to have better results although the number of samples is considerably decreased (especially for Egmond aan Zee).

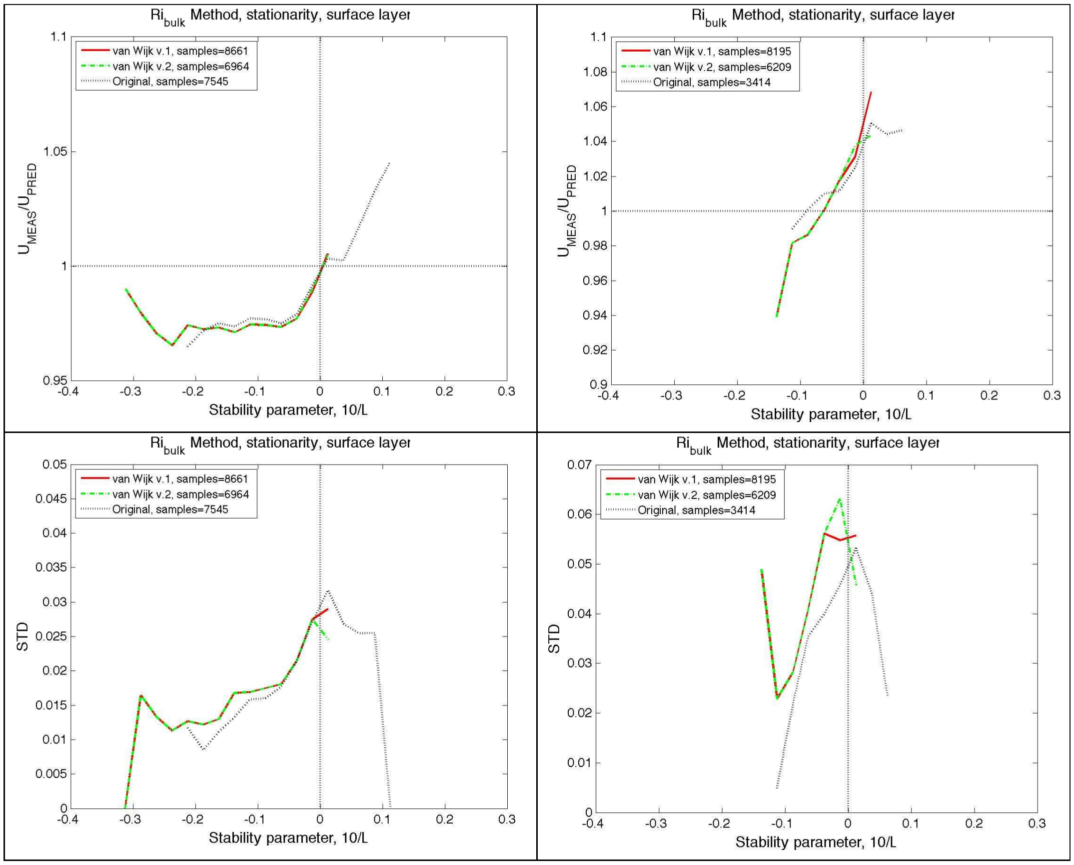

Figure 5.5: Influence of different Planetary Boundary Layer (PBL) height definitions on predicted wind speed at 90m in FINO-1 and 116m in Egmond aan Zee using Richardson Bulk Method. The results are shown in terms of average ratio of measured and predicted wind speed (top graphs) and standard deviation of this ratio (bottom graphs). The results are reported for relations (5.1) (labelled van Wijk v.1), relations (5.2) (van Wijk v.2) and relation (4.1) (Original). The assumption of surface layer equals to 10% of the PBL is taken for all cases. The virtual sea surface temperature Tv_{sea} is used as reference. On the left side the data from FINO-1 and on the right side Egmond aan Zee.

This analysis has shown how the effect of the height of z_s (if defined as proportional to the friction velocity) is not the only problem in the wind speed profile estimation, but the model itself has difficulties in calculating the wind speed, specifically in stable stratifications. Also the different behaviour shown by the model in the two offshore sites emphasises the limitation of the MO Similarity Theory. There are thus some parameters that are not considered (or wrongly treated) in the theory that play an important role in the wind profile definition.

5.3 Effects of Distance to the Coast and Wind Speed

Ri_{bulk} Method estimates the wind speed differently for FINO-1 and Egmond aan Zee (see for instance Figure 4.7). This different behaviour could be caused by dissimilar site conditions between the two offshore datasets. In this section, the different climatology of FINO-1 and Egmond aan Zee are investigated in details. The phenomena, for which the model is weakly able to estimate and simulate the flow condition, are presented in this part and an explanation is provided. In particular the relation between wind speed profile (and model wind speed prediction), distance from the coast and reference wind speed are analyzed. The reference wind speed is the speed at the lower level used by the model to estimate the wind speed at higher elevations. In this way the differences between the real airflow and the simulations can be shown. The data are filtered with only stationary filter firstly and then with both filters. The use of the surface layer filter decreases the number of samples considerably, especially at lower wind speeds the data are completely omitted (as can be noticed in Figure 5.14). When only the stationary filter is applied, the assumption made is that u_* is constant within the level of the highest anemometer for all the samples. Although this is not true, for research, it is interesting to see the effects of the flow when z_s height is not taken into account. The increased number of available samples helps to have a better statistic of the flow regime for various conditions. On the other hand, the use of surface boundary layer filter helps showing the effects of z_s height on the fetch analysis.

Figure 5.2 has shown that the use of different $T_{air\text{-}sea}$ changes the results considerably and the use of Tv_{sea} gives slightly better results. Hence the present analysis is mainly conducted using the Tv_{sea}. However some interesting results are compared with the ones in which T_{sea} is used. In the figures the results of the two sites are presented always with FINO-1 on the left and Egmond aan Zee on the right. Four different fetch conditions are reported in the graphs according to *WD*. In Figure 5.6 the definition of fetch is shown. In literature several definitions of fetch exist but the most common is the distance that the wind has flown above the sea before reaching the considered point. In this work, however, the fetch is defined as the distance from the coast of the considered offshore site and it is labelled as upwind fetch *X* if the wind reaches the site from the coast and downwind fetch *Y* if the airflow from the site reaches the coast.

Each dataset is sorted according to *WD* (measured at 90m in FINO-1 and 116m in Egmond aan Zee) in 12 sectors of 30°. The results are shown for four sectors and the *WD* indicated in the legend is the centre line of the reference sector. For example, the sector labelled 60˚ contains all the measurements (*u*, *T*, *RH*, etc.) that have *WD* between 45˚N and 75˚N. The graphs are organised for increasing upwind fetch. For FINO-1 the sectors are 180°N (45 km < *X* < 50 km and *Y* > 450 km), 150˚N (70 km < *X* < 100 km, *Y* > 450 km), 60˚N (130 km < *X* < 190 km, 80 km < *Y* < 100 km) and 240˚N (350 km < *X* < 400 km, *Y* > 100 km), while for Egmond aan Zee the sectors are 150°N (20 km < *X*< 30 km and *Y* > 300 km), 180˚N (30 km < *X* < 50 km, *Y* > 280 km), 240˚N (100 km < *X* < 150 km, 15 km < *Y* < 30 km) and 300˚N (*X* > 280 km, 20 km < *Y* < 30 km). The fetch distribution is different for Egmond aan Zee and FINO-1 (the nearest distances from the coast are around 18 km and 45 km respectively). Only for the direction 180˚N similar conditions can be found; but even for this *WD* the *Y* has different range, since in Egmond aan Zee there are fetches of 30 km while in FINO-1 only larger than 45 km.

Figure 5.6: Definition of upwind *X* and downwind *Y* distance to the coast.

Figure 5.7 shows the ratio u_{meas}/u_{pred} for varying *u* at the reference level (33m for FINO-1 and 21m for Egmond aan Zee) according to the four different *WD*. A general overestimation of the wind profile is present in FINO-1 and an underestimation in Egmond aan Zee. In both graphs the error decreases with increasing *u* and the error is high when *u* is lower than 8 m/s in FINO-1 and 5 m/s in Egmond aan Zee. For both offshore sites the very low wind speeds are difficult to estimate and considerably large errors are encountered. Increasing *u*, the error reduces first for higher *X* than for lower ones. The model describes the wind profile better for large fetches than for shorter ones.

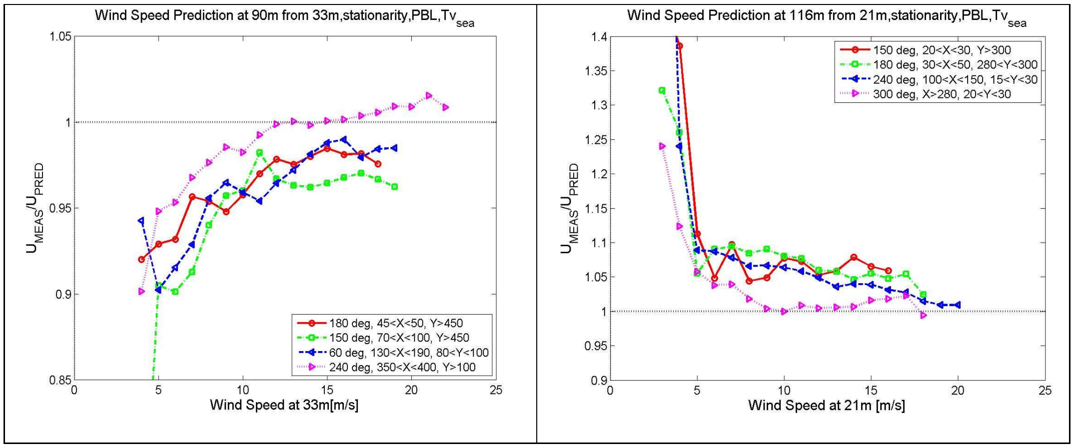

Figure 5.7: Wind speed prediction at 33m in FINO-1 and 116m in Egmond aan Zee with respect to reference wind speed *u* using Richardson Bulk Method. The results are reported only applying the stationary filter and with the virtual sea surface temperature Tv_{sea}. The legend in the graphs indicates the wind speed direction considered and the distance to the upwind (*X*) and downwind (*Y*) coast. Any considered wind direction has got a sector width of 30˚ centred on the indicated direction. On the left side the data from FINO-1 and on the right side Egmond aan Zee.

Figure 5.8 illustrates the wind profile with respect to the stability stratification using the same characteristic *WD*. FINO-1 has a flat wind speed profile for the unstable and very unstable conditions. This is slightly higher for large fetch conditions and lower when *X* is less than 100 km. The opposite happens for Egmond aan Zee; here the fetch dependence on wind shear is not clear for very unstable conditions while for unstable, near neutral and stable conditions such dependence on fetch is clearer. A small offset can be noticed in the wind shear between the directions with short fetch (150° and 180°) and the directions with large fetches (240° and 300°).

The wind shear increases with the stability and is proportional to the proximity from the coast in Egmond aan Zee while it seems inversely proportional in FINO-1. This interpretation is not straightforward since the direction 60˚N (in FINO-1) shows a lower wind shear. For Egmond aan Zee more is the distance from the coast more the time the fluxes have to bring the flow (and so the wind shear) to a near-neutral profile configuration. Hence, the flow starts with larger velocity gradient, due to considerable air temperature stratification, and with passing time this stratification reduces, due to thermal and mechanical mixing and the ratio between the wind speeds decreases. The situation is different For FINO-1; for large fetches there is a higher wind shear probably due to increasing in wave height. The airflow, for direction 240˚N comes from open sea with *X* of more than 350 km and it goes towards open sea (*Y* more than 100 km). So the flow has time to interact with the seawater and create high waves (and so higher roughness length) and hence higher wind shear. Moreover, the research platform FINO-1 is placed far from the coast where the seabed is about 30 m and so there is not the effect of wave breaking due to low depth of the sea. In contrast the met mast of Egmond aan Zee is closer to the Dutch coast and the seabed is about 18 m. This could explain the differences in wind speed profile between the two sites. Indeed, if the very high fetch (240˚N) is excluded from the analysis, FINO-1 shows (in the range near-neutral and very stable) a decrease in wind shear when *X* increases.

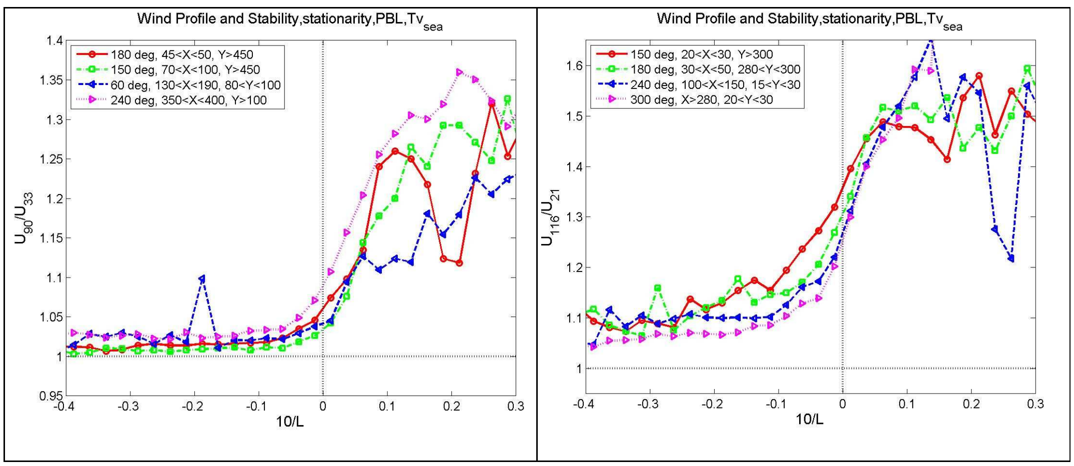

Figure 5.8: Wind speed profile with respect to stability parameter *10/L* using the Richardson Bulk Method. The results are reported only applying the stationary filter and with the virtual sea surface temperature Tv_{sea}. The legend indicates the wind speed direction considered and the distance to the upwind (*X*) and downwind (*Y*) coast. Any considered wind direction has got a sector width of 30˚ centred on the indicated direction. On the left side the data from FINO-1 and on the right side Egmond aan Zee.

Similarly, the situation reported in Figure 5.9 tells how the model estimates the wind speed at higher elevations using the information at the reference low level according to stability distribution and distance from the shore. The Ri_{bulk} Method does not work properly in all directions for FINO-1 and neither for the stability classification. The error is larger (as seen) in stable conditions and for lower fetches. For Egmond aan Zee the model underestimates the wind shear in unstable, near-neutral and stable stratifications and for very stable conditions the model overestimates the wind speed.

As explained in section 5.1, the effect of using Tv_{sea} is an increase in temperature difference. This means that when the stratification is unstable the model considers the flow very unstable and when the flow is stable (or very stable) the airflow is considered less stable or even unstable. Hence, in general, a lower wind shear is defined. This explains the behaviour of the wind speed prediction in the graphs. This effect creates large underestimation in near-neutral and stable conditions (around 0.1) in Egmond aan Zee. The large *X* directions show underestimation while smaller *X* almost match the measurements. This can underline again the fetch dependence of the flow. For large fetches the flow has the time to reach the new wind profile configuration in equilibrium with the new conditions of roughness length and $T_{air\text{-}sea}$. This new configuration is close to a near-neutral profile. Since Egmond aan Zee is closer to the coast, this effect is more evident compared to FINO-1. Hence for both datasets it is clear that the fetch distribution affects the model prediction. Alternatively, the geography of the site influences the characteristics of the flow regime. The distance from the coast, both upwind and downwind, affects the flow development due to the land-sea discontinuity and growth of wind waves.

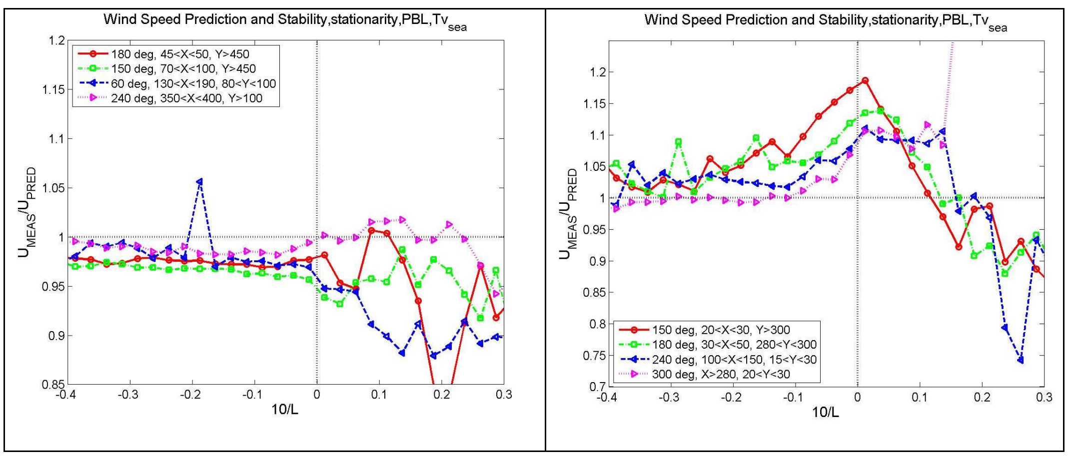

Figure 5.9: Wind speed prediction at 33m in FINO-1 and 116m in Egmond aan Zee with respect to the stability parameter *10/L* using Richardson Bulk Method. The results are reported only applying the stationary filter and with the virtual sea surface temperature Tv_{sea}. The legend indicates the wind speed direction considered and the distance to the upwind (*X*) and downwind (*Y*) coast. Any considered wind direction has got a sector width of 30˚ centred on the indicated direction. On the left side the data from FINO-1 and on the right side Egmond aan Zee.

Figure 5.10 and Figure 5.11 show the relation between *10/L* and *u*. For these graphs the results are plotted both using T_{sea} and Tv_{sea}. This is because, for this analysis, the results change considerably when a different definition of $T_{air\text{-}sea}$ (air temperature at air-sea interface) is used, especially for Egmond aan Zee. Indeed, when Tv_{sea} is applied in Egmond aan Zee, the graphs show an unforeseen increase in wind shear (almost for all stratifications) when *u* decreases, while the contrary can be observed in FINO-1. When T_{sea} is considered, the two offshore databases have similar results. The wind shear is uniform in unstable and vey unstable stratifications for any wind speed class. For stable conditions the wind shear increases with respect to the reference wind speed, higher the wind speed larger the wind shear. Hence the wind shear depends on the mechanical momentum exchanges. The dependence of wind shear on mechanical momentum was expected since for near-neutral and stable conditions the thermal effects are less important. When Tv_{sea} is applied the behaviour of Egmond aan Zee is not easily explained. It is not clear why only for this dataset the wind shear decreases with increasing u and why it is different from FINO-1. The results with both Tv_{sea} and T_{sea} have been plotted because it is important to show how the definition of $T_{air\text{-}sea}$ can influence the results.

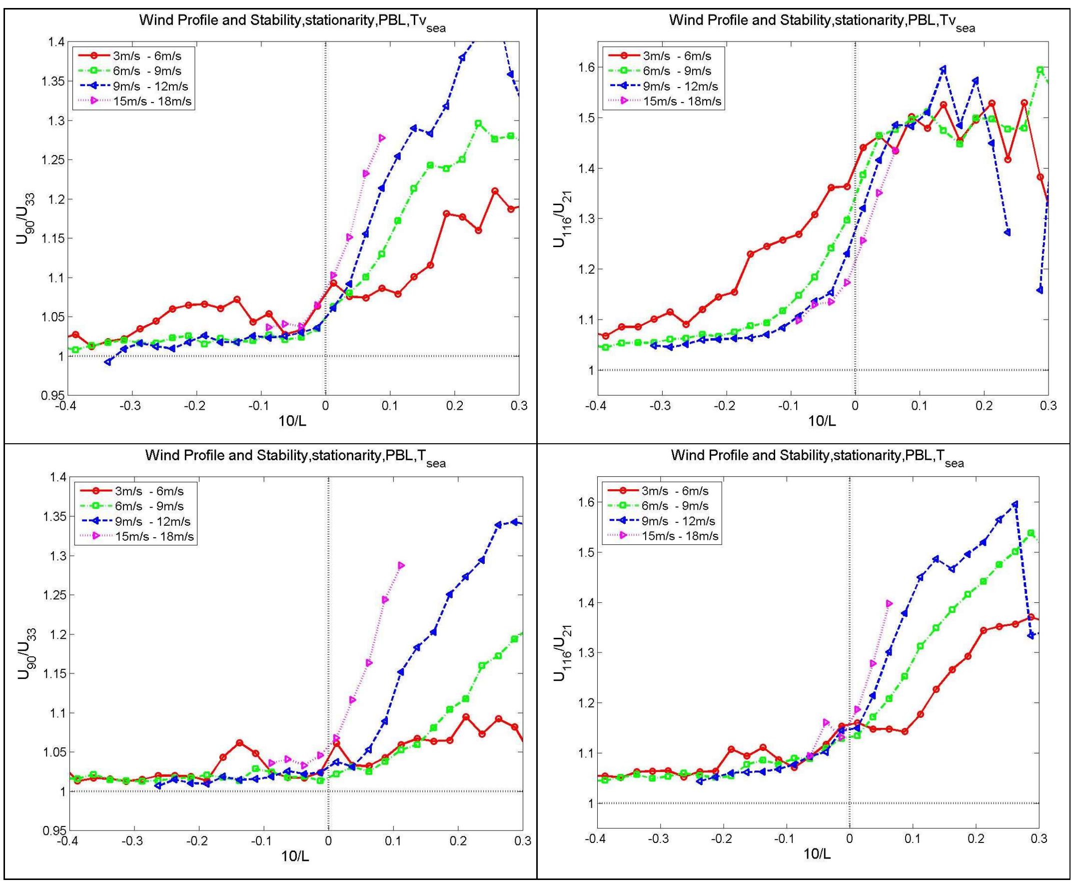

Figure 5.10: Wind speed profile with respect to stability parameter *10/L* and reference wind speed u (measured at 33m in FINO-1 and 21m in Egmond aan Zee), with only stationary filter and using the Richardson Bulk Method. The legend indicates the range of the reference wind speed. In the top graphs the results are shown with virtual sea surface temperature Tv_{sea} and in the bottom with absolute sea surface temperature T_{sea}. On the left side the data from FINO-1 and on the right side Egmond aan Zee.

This behaviour is also indicated in Figure 5.11 where the ratio u_{meas}/u_{pred} is shown for both Tv_{sea} and T_{sea}. The graphs show that decreasing u the model error increases. The use of Tv_{sea} shows differences between FINO-1 and Egmond aan Zee, the first shows overestimation and the latter underestimation. The situation is likely the same for both databases when the T_{sea} is used. Larger is the wind speed class larger is the overestimation. Looking carefully at the graphs of Figure 5.11, for the speed class 15 - 18 m/s the results are similar (almost identical in same cases) to the graphs shown with both stationary and surface layer filters in Figure 5.1 and Figure 5.2. This means that for large u the condition of surface layer is accomplished while for low u not. These results explain that moving away from the condition of surface boundary layer the MO Similarity Theory slowly becomes less reliable and this condition is mostly based on u, especially in stable conditions.

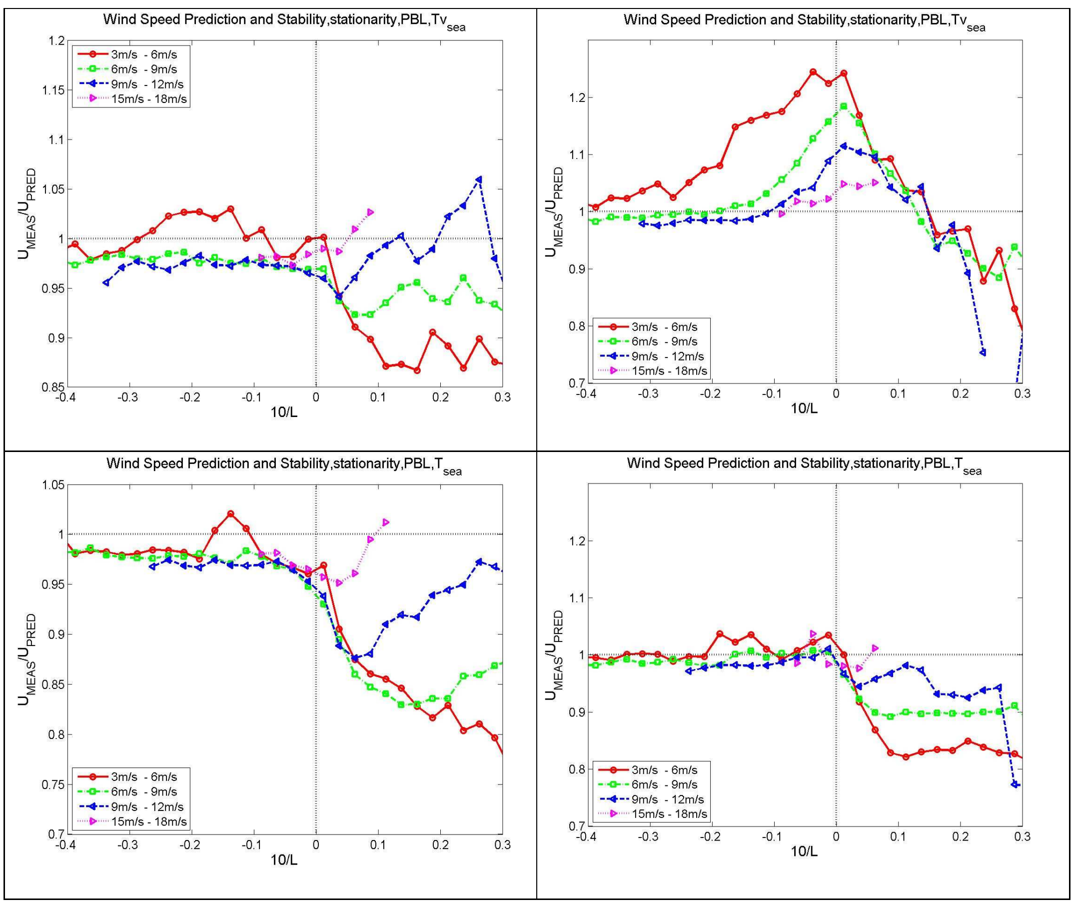

Figure 5.11: Wind speed prediction with respect to dimensionless stability parameter *10/L* and reference wind speed *u* (measured at 33m in FINO-1 and 21m in Egmond aan Zee), with only stationary filter and using the Richardson Bulk Method. The legend indicates the class of the reference wind speed. In the top graphs the results are shown with virtual sea surface temperature Tv_{sea} and in the bottom with absolute sea surface temperature T_{sea}. On the left side the data from FINO-1 and on the right side Egmond aan Zee.

Figure 5.12 and Figure 5.13 show the relation between *10/L* and *u* for two different fetch conditions. The *WD* of 180°N, for both sites, represents the short *X* while 240°N for FINO-1 and 300°N for Egmond aan Zee represent the large *X* distance from the coast. These two figures have been selected to show the characteristics reported in Figure 5.10 for all the fetches and seeing, in this case, the differences with respect to fetch distance.

The graph of Egmond aan Zee is similar to the one shown in Figure 5.10, while for FINO-1 the low wind speeds report a lower wind shear. For very stable conditions, however, the lowest wind range is not big enough to let the waves growing and hence the roughness length is low. The flow has more time when the wind speed is low to adapt to the new lower boundary condition (the sea) when passing from land to sea and thus the wind shear decreases. This behaviour is common for both sites but the gap between the three high velocities and the lowest one is evident only for FINO-1.

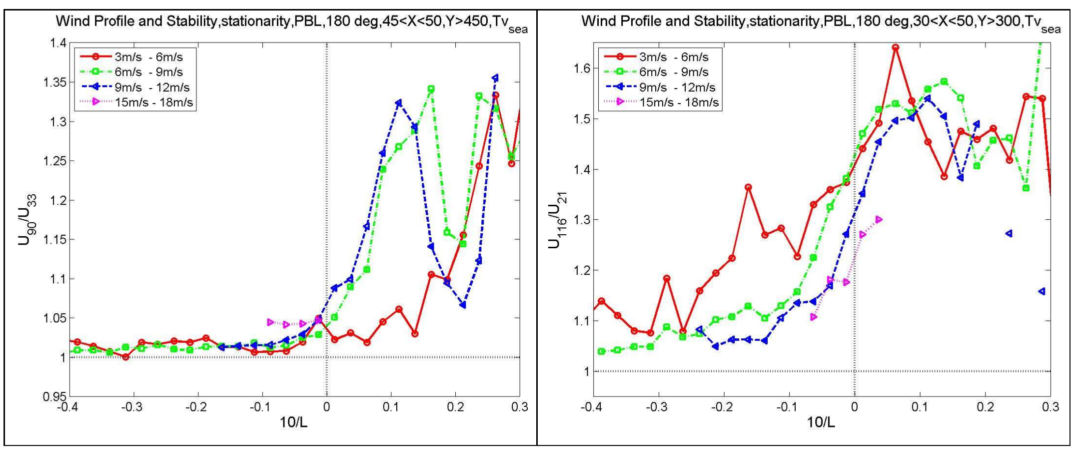

Figure 5.12: Wind speed profile with respect to dimensionless stability parameter *10/L*, using the Richardson Bulk Method. The results are reported only applying the stationary filter and with the virtual sea surface temperature Tv_{sea}. The results are shown for the wind direction 180˚ where the upwind (*X*) fetch is low in both sites. The legend indicates the class of the reference wind speed. On the left side the data from FINO-1 and on the right side Egmond aan Zee.

Figure 5.13 shows that the wind shear is slightly lower for high wind speeds than in Figure 5.12. The graphs show also that the difference between wind classes is to some extent lower than in the graphs of Figure 5.12. In these conditions the flow has the space (and time) to let the waves grow and consequently the wind shear is high also for low *u*.

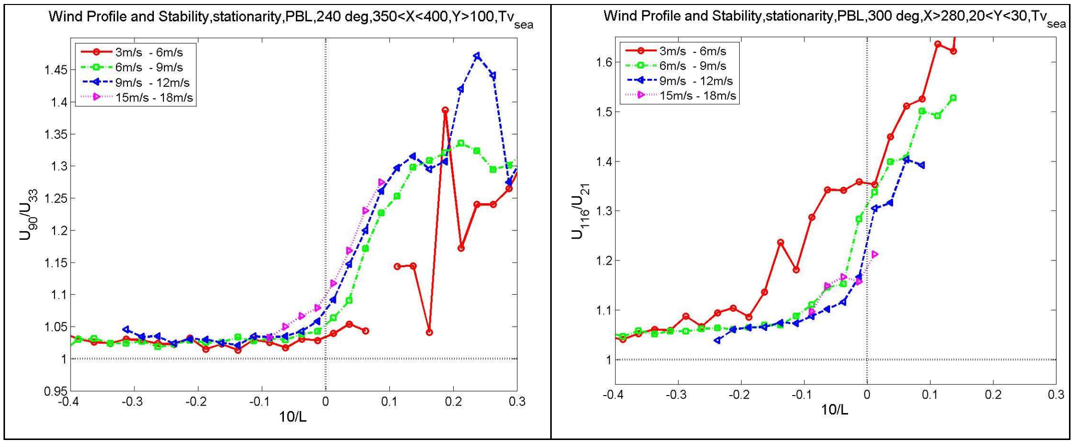

Figure 5.13: Wind speed profile with respect to dimensionless stability parameter *10/L*, using the Richardson Bulk Method. The results are reported only applying the stationary filter and with the virtual sea surface temperature Tv_{sea}. The results are shown for the wind direction 240˚ for FINO-1 and 300˚ for Egmond aan Zee, where the upwind (*X*) fetch is high in both sites. The legend in the graphs indicates the range of the reference wind speed. On the left side the data from FINO-1 and on the right side Egmond aan Zee.

The fetch analysis continues using both stationary and surface layer filters to show the effects of surface boundary layer on the results. Figure 5.14 shows the ratio u_{meas}/u_{pred} for varying u at the reference level (33m for FINO-1 and 21m for Egmond aan Zee) according to four different *WD* (related to *X* distance from the coast). These graphs are similar to Figure 5.7, but applying the surface boundary layer filter. The filter, indeed, excludes the data with lower u such as less than 12 m/s at FINO-1 and 15m/s at Egmond aan Zee, but the results follow the same trend. The surface boundary layer filter maintains the same flow characteristic with respect to the shore distance for large u and excludes the values for low u.

Figure 5.15 gives the wind speed profile for the two offshore sites as ratio lower and higher level wind speeds with respect to the stability parameter *10/L* and using both stationary and surface layer filters. The graphs report the wind shear according to *X* distance to the coast as shown in Figure 5.8. The graphs show similar results to those given in Figure 5.8. However, here it is less evident the difference in wind shear according to fetch. All the lines are close to each other around near-neutral conditions. Especially for Egmond aan Zee the points follow almost the same path. The filter thus reduces the coast influence. This means that the flow develops in the same way according to *X* distance from the coast. The filter selects the measurements with higher u_* hence the buoyancy term plays a smaller role than the mechanical momentum exchange. Reducing the effects of the buoyancy term means a reduction in air mixing. The flow of information from the lower levels to the higher ones decreases. In this way, the airflow tends to keep its structure and the wind shear is similar for different fetch conditions.

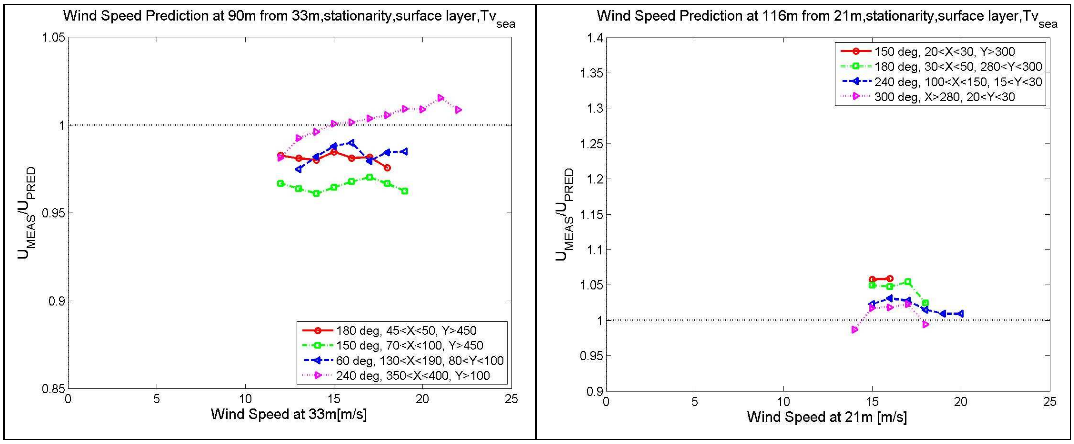

Figure 5.14: Wind speed prediction at 33m in FINO-1 and 116m in Egmond aan Zee with respect to the reference wind speed *u* using Richardson Bulk Method. The results are reported applying both the stationary and surface layer filters and with the virtual sea surface temperature Tv_{sea}. The legend in the graphs indicates the wind speed direction considered and the distance to the upwind (*X*) and downwind (*Y*) coast. Any considered wind direction has got a sector width of 30˚ centred on the indicated direction. On the left side the data from FINO-1 and on the right side Egmond aan Zee.

The airflow behaviour described in Figure 5.15 reflects on the results of Figure 5.16, which tells how the model evaluates the wind speed with respect to *10/L* and *X*. Figure 5.16 is similar to Figure 5.9, but here both filters are applied. However, the results are different since the model estimates more accurately the wind speed profile when both filters are applied. This is valid for both FINO-1 and Egmond aan Zee. The large error (seen in Figure 5.9) is absent and in particular for Egmond aan Zee the error decreases and the differences with respect to the fetch are not evident.

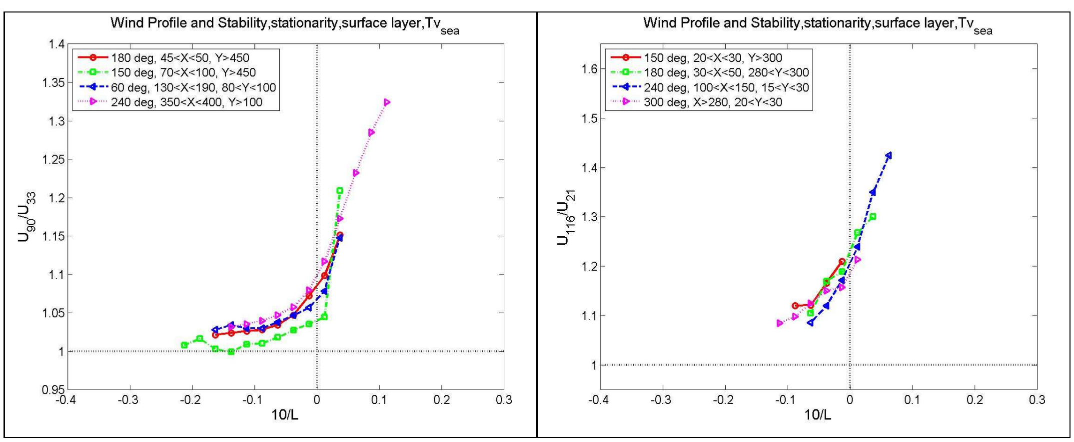

Figure 5.15: Wind speed profile with respect to stability parameter *10/L* using the Richardson Bulk Method. The results are reported applying both stationary and surface layer filters and with the virtual sea surface temperature Tv_{sea}. The legend indicates the wind speed direction considered and the distance to the upwind (*X*) and downwind (*Y*) coast. Any considered wind direction has got a sector width of 30˚ centred on the indicated direction. On the left side the data from FINO-1 and on the right side Egmond aan Zee.

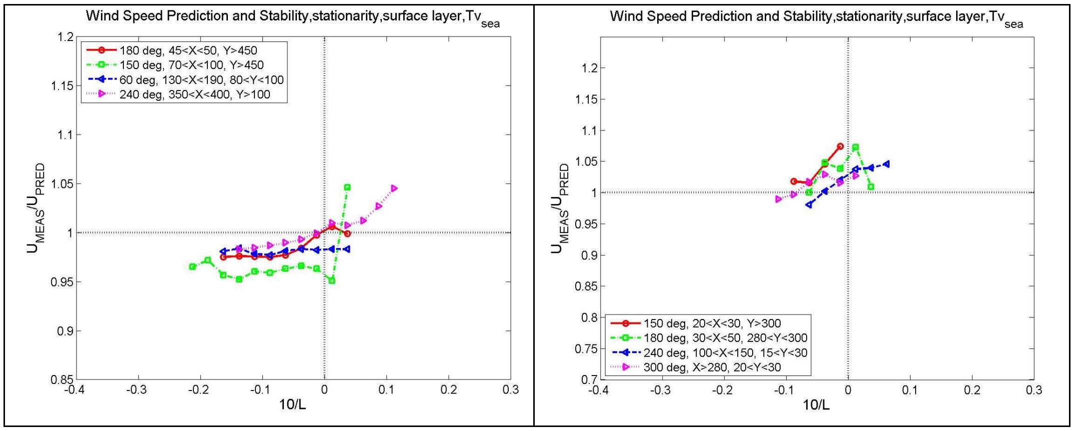

Figure 5.16: Wind speed prediction at 33m in FINO-1 and 116m in Egmond aan Zee with respect to the stability parameter *10/L* using Richardson Bulk Method. The results are reported applying the stationary and surface layer filters and with the virtual sea surface temperature Tv_{sea}. The legend indicates the wind speed direction considered and the distance to the upwind (*X*) and downwind (*Y*) coast. Any considered wind direction has got a sector width of 30˚ centred on the indicated direction. On the left side the data from FINO-1 and on the right side Egmond aan Zee.

Seen the climatology for these two offshore sites and how the model simulates the different phenomena, it is important to summarize the characteristics of the Ri_{bulk} Method:

- The use of Tv_{sea} reduces the wind shear estimation giving better results in offshore sites with large fetch distributions, like FINO-1.
- The behaviour of FINO-1 and Egmond aan Zee is different as far as it concerns the parameters *10/L* and *u*. In near-neutral and stable stratifications the wind shear increases with increasing *u* in FINO-1 while it decreases in Egmond aan Zee.
- For very unstable stratifications, the graphs show slightly dependence on fetch conditions.
- In near neutral, stable and very stable conditions the fetch dependence is evident.
- The fetch dependence reduces when the surface boundary layer filter is applied.
- The wind speed estimation error increases with decreasing reference *u*, especially in stable conditions.

Chapter 6

WEATHER FORECAST MODEL ANALYSIS

In this chapter the Monin-Obukhov Similarity Theory is applied to the database provided by the weather forecast model COSMO-EU, used by the German Facility Centre of the Deutscher Wetterdienst. The results are compared with the measurements at FINO-1. To this aim the hourly time series of DWD is equal to the FINO-1 10-min time series for the years 2005-2006. Only the measurements taken at the same period of time in both databases are considered. With this condition the number of samples is 5030 for DWD and 27328 for FINO-1. It is important to comprehend how the remote sensing data (and/or weather model data) could be used, especially for offshore wind energy applications. The following analyses will be conducted using the Ri_{bulk} Method with Tv_{sea} and both stationary and surface layer filters.

6.1 DWD Analysis

In this section the stability analysis of the DWD dataset and the comparison with FINO-1 database are carried on. The same stationary and surface layer filters are applied to both datasets. The same period of time is used; this means that year, month, day and hour coincide for any sample. The data presented are thus the 10-min results for FINO-1 and 1-hour for DWD. To compare the data of DWD and FINO-1, the model wind speeds have been interpolated since no values were present at 33m and 90m levels. The samples decrease considerably in DWD when both filters are applied and especially when the stationary filter is present, because the difference between 1 sample and the proceedings or the followings is, in general, considerably high since they are 1-hour average values.

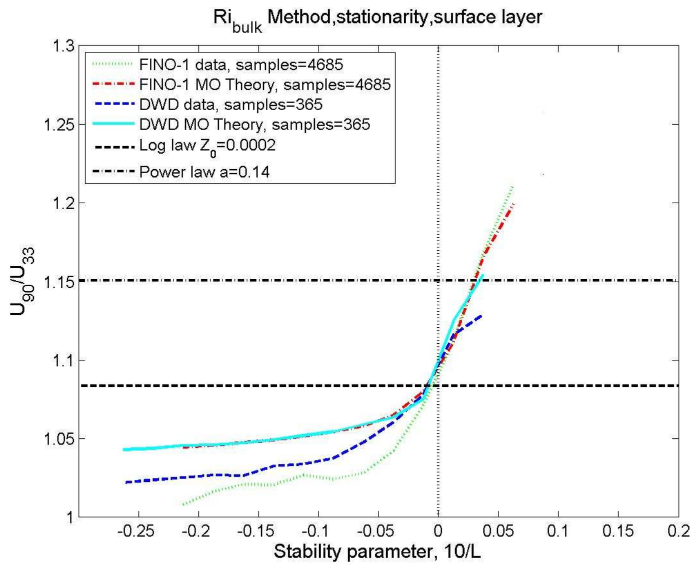

Figure 6.1: Wind speed profile at FINO-1 location using measurements (10-min average) and DWD model data (1-hour average). The line labelled “FINO-1 data” represents the measurements of the offshore database while “FINO-1 MO Theory” represents the results of applying the Monin-Obukhov Similarity Theory to FINO-1 database. The line labelled “DWD data” represents the results for the weather forecast model, while “DWD MO Theory” represents the results of applying the Monin-Obukhov Similarity Theory to the DWD database. The Richardson Bulk Method is used with stationary and surface layer filters.

Figure 6.1 shows the wind speed ratio between 90m and 33m as function of *10/L* at FINO-1 location. In this graph different results are plotted. The line labelled “FINO-1 data” takes the measurements of the research platform (FINO-1), the one with “FINO-1 MO Theory” indicates the use of MO Similarity Theory using the platform data, “DWD data” takes the measurements of the weather forecast database and “DWD MO Theory” indicates the use of MO theory applied to the DWD database. The wind speed profile calculated with the MO theory does not fit the wind profile estimated with the COSMO-EU model in unstable and very unstable conditions, while for near-neutral and stable conditions it does fit. The DWD wind shear matches very well in near-neutral conditions and good in stable ones for both FINO-1’s measurements and MO theory. In unstable and very unstable conditions the DWD model shows a smaller wind shear with respect to the theory but a higher one compared to the 10-min FINO-1’s measurements. The wind shear is generally closer to the FINO-1’s measurements so that the DWD model defines the wind shear better than the MO theory.

It can be noticed that the theory predicts the samples in DWD’s dataset better than FINO-1’s. Comparing Figure 6.1 and Figure 6.2, it is clear that when a simpler model is applied the estimation accuracy decreases. The difference between the theory and DWD model in terms of weighted average error is 0.8% and the standard deviation is about 0.6%.

The results of this analysis are important not only from a theoretical point of view, but more from a practical one. Often it happens that a weather (satellite) model or a remote sensing measurement gives the parameters at one level but one might want to know the wind speed profile at different levels. The MO theory can in this case estimate u_{pred} for other levels of interest and the results can be considered reliable.

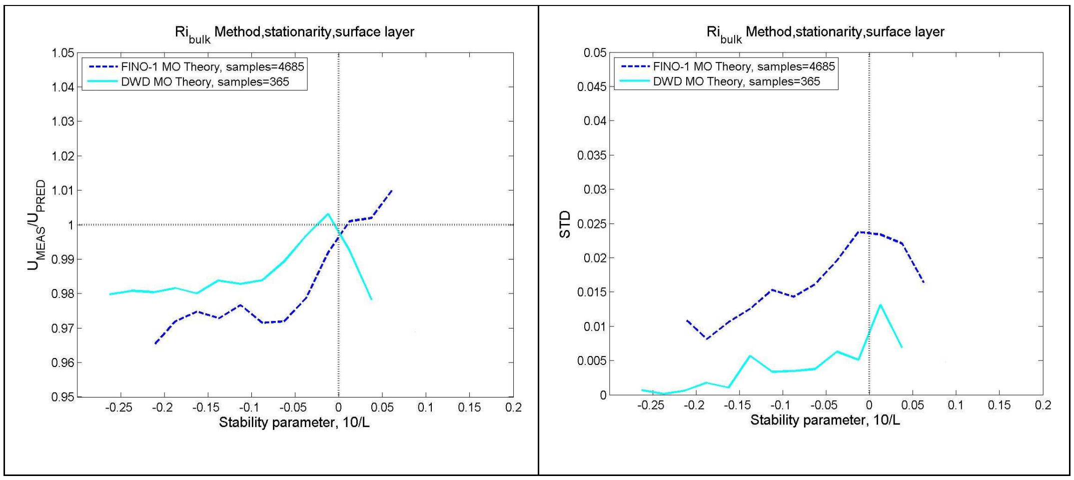

Figure 6.2: Ratio of measured and predicted wind speed at 90m (left) and standard deviation of this ratio (right) at FINO-1 location using measurements and DWD model data. For both databases the wind speed at 33m is used to predict the wind speed at 90m. The line labelled “DWD MO theory” represents the results for the weather forecast model applying the Monin-Obukhov theory, while “FINO-1 MO Theory” represents the results of applying the theory to the FINO-1 database. The Richardson Bulk Method is used with stationary and surface layer filters.

6.2 Sea Surface Temperature Analysis

For wind energy applications and in general for research purposes, specific sea measurements are not available in the sites of interest. Commonly the wind speed can be found thanks to oil platforms far away from the coast that use the wind speed for helicopter landing or thanks to ships that provide voluntary meteorological information (like in the KNMI database); but the measurement of the sea surface temperature and even the air temperature and humidity over sea are not routinely made. For this reason it is relevant to investigate the use of remote sensing data or weather forecast models in order to integrate the real measurements. This section combines the *u* measurements from FINO-1 with the *SST*, *T* and *RH* from the DWD model. The *SST* is taken daily from the NOAA database [27] and it comes from satellite measurement. The value of *SST* is used as input to the DWD's COSMO-EU model. *T* is an output of DWD model and *RH* is derived from the dew point at 2m and assumed being the relative humidity at 33m. The time resolution for both *T* and *RH* is 1-hour while 10-min for all FINO-1's measurements: at the same hour the code uses one value of DWD *T* while six FINO-1's measurements, i.e. the same *T* is associated to six different wind measurements.

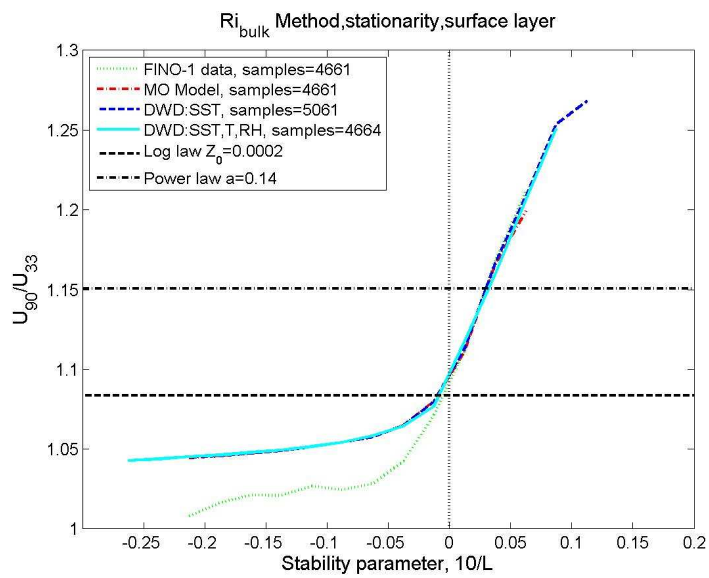

Figure 6.3: Wind speed profile at FINO-1 location using measurements and DWD model data, the lines labelled "DWD" represent the results where one or more variables of FINO-1 have been substituted with DWD database. The Monin-Obukhov model used is the Richardson Bulk Method with stationary and surface layer filters.

Figure 6.3 shows the wind speed ratio between 90m and 33m as function of stability parameter *10/L* at FINO-1 location. The line labelled "FINO-1 data" takes all measurements of FINO-1, the one with "MO Model" indicates the use of MO similarity theory using platform data, "DWD *SST*" and "DWD *SST*, *T*, *RH*" indicate respectively the use of *SST* and *SST*, *T* and *RH* from DWD database and the *u* from FINO-1 database to estimate the wind profile. The graphs indicate that, whatever set of data is used, the definition of the wind shear is the same using the MO Similarity Theory. This is what was expected since the wind shear is fully determined by the term $\Psi(10/L)$ because the roughness length slightly changes accordingly to

Charnock's relation. However the theory does not match the FINO-1's measurements especially in unstable conditions.

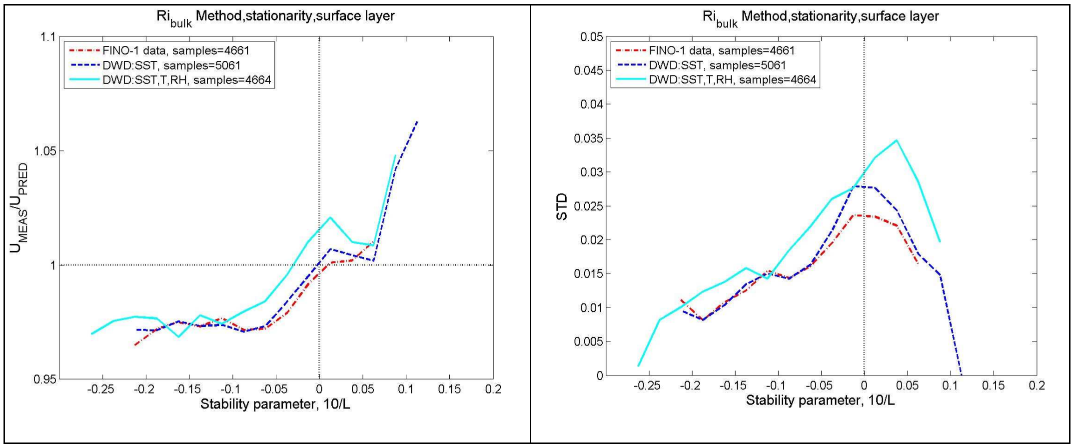

Figure 6.4: Ratio of measured and predicted wind speed at 90m (left) and standard deviation of this ratio (right) at FINO-1 location using measurements and DWD model data. For both databases the wind speed at 33m is used to predict the wind speed at 90m. "FINO-1 data" represents the results of applying the Monin-Obukhov theory to the FINO-1 database. The lines labelled "DWD" represent the results where one or more variables of FINO-1 have been substituted with DWD model data. The Monin-Obukhov model used is the Richardson Bulk Method with stationary and surface layer filters.

Figure 6.4 shows the predicted wind speed and its standard deviation versus stability for the different combinations of data. The dashed blue line reports that the estimation using the *SST* from the meteorological database does not change considerably the results (only a small offset in the mean value and 0.05% in standard deviation, both around the near-neutral condition). This is an important result for two main reasons: the possibility to use remote sensing data to estimate *SST* and its effects on the Ri_{bulk} Method. The possibility of using the *SST* from a model (or satellite remote sensing) solves several logistic problems in the campaign of data acquisition in terms of time (model databases are ready to be used and have long time period of available data) and cost. Submerging sensors are expensive requiring experts for their installation and maintenance. The second important point concerns the way of measuring *SST*. This is a difficult parameter to measure because it is really difficult to catch the real absolute temperature in the first millimetres of seawater or air (i.e. exactly at the interface between the two media, see Figure 2.1). The results show that measuring at some meters below the sea level (FINO-1 sensor) or using a remote sensing measure (DWD) does not give any particular disadvantage. Since there is not a large difference in the results between 1-day resolution *SST* of

DWD and 10-min *SST* of FINO-1, it can be concluded that time resolution for *SST* is not relevant. If the time resolution is not important, also the cool-skin and warm layer[2] effects (see [16] and [26]) appear to be unimportant to estimate the wind speed profile. Indeed cool-skin and warm-layer act on a small time scale because they are influenced by factors (like solar irradiation, precipitation and wind speed) that have a resolution of few hours. Moreover the cool-skin and warm-layer effects can alter the temperature within 1 degree (see [16]). Such temperature difference is already present between DWD's *SST* and FINO-1's (see Figure 6.5), but the results indicate that this is not enough to change the estimation of the wind speed profile.

In Figure 6.4 the light blue line indicates the results with FINO-1's wind speed and *SST*, *T* and *RH* from DWD. The results are reasonably satisfying except for an offset in near-neutral and unstable conditions. The standard deviation is on average slightly higher. These results can be explained because the correlation of the two datasets is high for the parameters *SST* and *T*, as shown in Figure 6.5. In these graphs an offset can be appreciated between the two *SST* and the two *T*. For *SST*, DWD has higher values while for *T* generally lower. It means that when both *SST* and *T* are taken from DWD database, the average temperature difference (the $\Delta\theta_v$ term in relation (2.18)) is smaller, hence the model calculates a different stability stratification, i.e. always less stable. This effect explains the difference in number of samples between the results using all the data from FINO-1 and the results with DWD *SST*. A smaller temperature difference produces a higher u_*, if the same u is considered, and thus higher surface boundary layer height (see explanation in section 5.1).

In Table 6.1 the results are quantified in terms of weighted average (the average of each bin times the number of samples) of u_{meas}/u_{pred} (in the table AVG) and the weighted average of the standard deviation (STD). The results show a good estimation of the wind speed; but it must be taken into account that overestimations are averaged with underestimations. This means that these values are not constant and the effects on loads calculations and power yield should not be taken using the average. Indeed it seems that the average becomes better applying the DWD parameters. The weighted mean of the standard deviation is instead a clear index of the variation of the wind speed prediction and it shows that on average the estimation loses accuracy, although this change is less than 0.4% between FINO-1 and DWD (with *SST*, *T* and *RH*). Also quantitative the use of *SST*, *T* and *RH* from DWD does not alter significantly the results.

[2] The cool-skin and warm layer effects are two phenomena that happen in the first layers of seawater. When the wind blows, for effect of heat exchange between air and water the temperature in the first millimeters tends to reduce, while for effect of solar irradiation a slightly larger layer tends to increase its temperature. The two effects always compensate but this behavior is not constant and difficult to model (see [16]). Hence the temperature measured at levels below the mean seal level is not the real sea surface temperature.

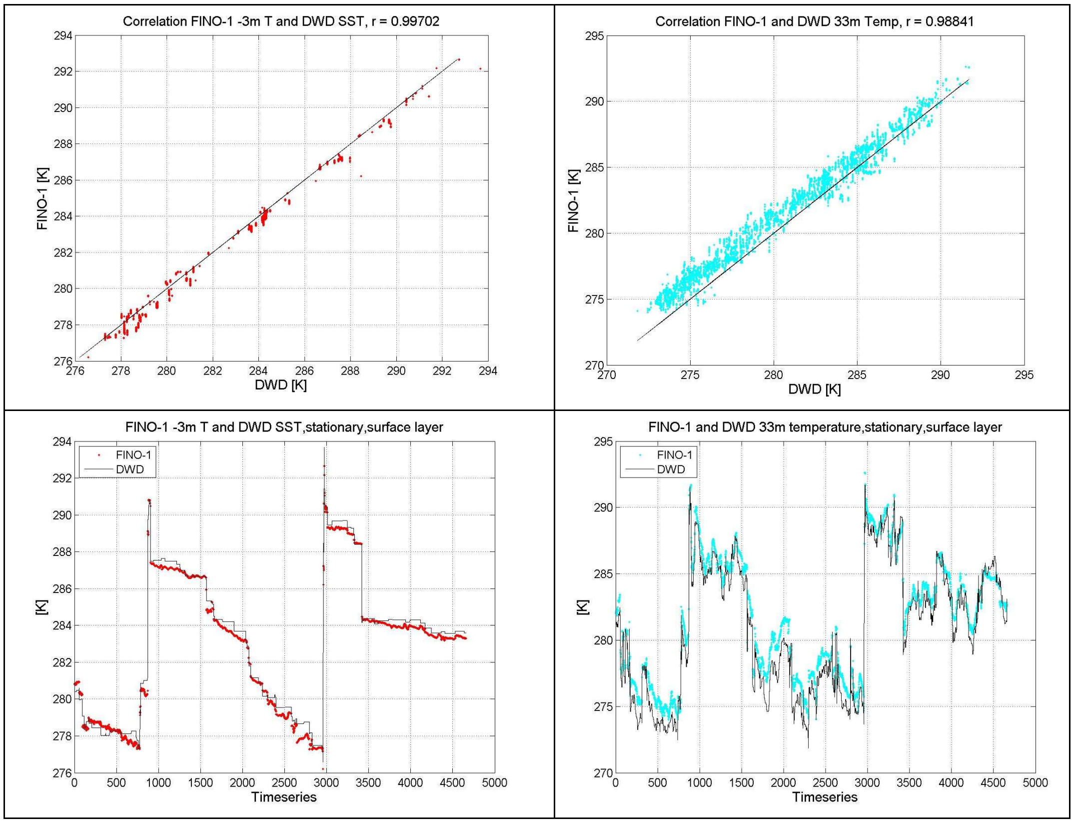

Figure 6.5: Correlation between FINO-1 and DWD air temperature and *SST*. In the top graphs the correlation between -3 m sea temperature of FINO-1 and DWD's SST (left) and the correlation between 33 m air temperature for FINO-1 and DWD (right). The sample correlation coefficient *r* is indicated in the titles of the top graphs. The timeseries of *SST* and 33m air temperature are shown in the bottom graphs.

	FINO-1: *u, T, RH, SST*	FINO-1: *u, T, RH* DWD: *SST*	FINO-1: *u* DWD: *SST, T, RH*
AVG	0.988	0.991	0.997
STD	0.021	0.024	0.025

Table 6.1: Values of weighted average of the bin error and weighted average of the standard deviation for the three different combinations of *SST*, air temperature and relative humidity.

Knowing the frequency of atmospheric stratification is very important for a good wind assessment of an offshore site. It is important to see how model parameters influence the frequency of occurrence for a specific site (in this case for FINO-1). Figure 6.6 shows the comparison between the frequency of occurrence with the measurements from FINO-1 and the one with *SST*, *T* and *RH* from DWD. These graphs are an expression of the larger temperature difference just described. A larger temperature difference indicates more unstable conditions. So the number of near-neutral conditions decreases with respect to FINO-1 measurements when DWD data are used. (Note: the graph with FINO-1 data is not the same of Figure 4.1, because the timeseries used is different).

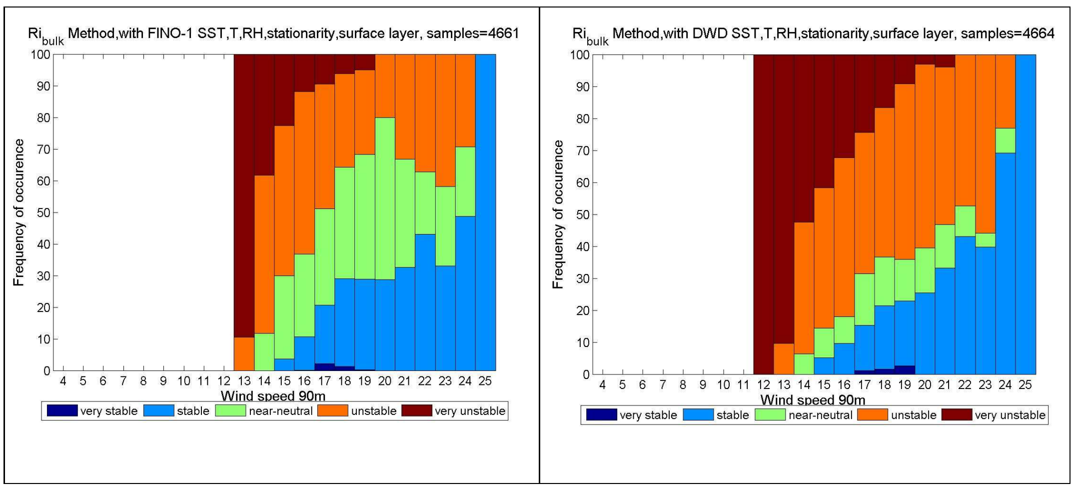

Figure 6.6: Frequency of occurrence of atmospheric stratifications at FINO-1 location using measurements (left) and DWD model data (right). The Monin-Obukhov model used is the Bulk Richardson Method with stationary and surface layer filters.

Chapter 7

CONCLUSIONS AND RECOMMENDATIONS

A few conclusions can be drawn from the analyses performed in this report about the offshore wind assessment in the North Sea using the Monin-Obukhov Similarity Theory:

- The applicability of the Monin-Obukhov Similarity Theory is site dependent. This theory shows different results and dissimilar behaviour for the two offshore sites and these differences are relevant for all the five methods to estimate the Obukhov length. This underlines what found in literature, i.e. dissimilar results for different sites. This means that even for the same sea (in this case the North Sea) each site has its own wind characteristics that are not well estimated by means of Monin-Obukhov Similarity Theory.

- The validity of the Monin-Obukhov Similarity Theory is based upon the assumption of stationary fluid (not changing in time) and surface layer (friction velocity constant). When these assumptions are not fulfilled the error in estimating the wind speed profile increases. This is not suitable because the flow is often not stationary and mostly the surface boundary layer height is lower than the highest level of interest.

- The Richardson Bulk Method gives better results than the other four methods. Except for the Sea Temperature Profile Method, all the other methods give less accurate results and hence they should not be used to investigate the wind profile in offshore conditions.

- The Richardson Bulk Method turns out to be sensitive to the air temperature definition. The results change considerably as function of the air temperature (absolute, virtual or potential temperature). Implementation of virtual potential temperature has the most reliable results.

- The Richardson Bulk Method is also sensitive to the sea surface temperature definition. Virtual temperature and absolute temperature give different results in both datasets and in particular for Egmond aan Zee. However, from a consistence point of view and from the results, the virtual sea surface temperature should be applied when the Richardson Bulk Method is used.

- The way of measuring the sea surface temperature is not relevant. The model gives slightly different results when the sea surface temperature is taken from the satellite with 1-day resolution or from the submerged sensor with 10-min resolution. Hence the warm-layer and cool-skin effects do not seem to play a role in the wind speed profile estimation.
- The Richardson Bulk Method shows a strong dependence on the reference wind speed: high wind speed improves the prediction. Generally a good precision in wind speed estimation is obtained for wind speed higher than the offshore wind turbine rated wind speed.
- The Richardson Bulk Method shows fetch dependence acting differently with respect to fetch distribution in the two sites. However, this dependence reduces when both stationary and surface boundary layer filter are applied. This shows that the surface boundary layer height plays an important role in the transition of the wind speed profile from land characteristics to sea ones.
- The weather forecast model COSMO-EU (provided by the Deutscher Wetterdienst DWD) gives promising results and it could be a good tool in offshore wind assessment. As database, the COSMO-EU model can be used for feasibility studies of prospective offshore wind farms. As implementing datasets, it can be used to integrate missing measurements from databases.

The Monin-Obukhov Similarity Theory in general and the Richardson Bulk Method in particular have shown difficulties in estimating the offshore wind speed profile. Hence, it is reasonable to conclude that the Monin-Obukhov Similarity Theory does not pick up all the important parameters influencing the offshore wind profile. Few recommendations can be provided:

- The site dependence could depend on the fetch distribution which is specific per each site. It is recommended a further analysis of the fetch conditions, possibly using databases with similar distance from the coast.

- The model shows wind speed dependence. An indication is thus to focus on the dependence of the Monin-Obukhov Similarity Theory on the wind speed in particular in near-neutral and stable conditions in order to tune the model to the real airflow conditions.
- The use of models different from the Monin-Obukhov Similarity Theory has to be carried on and validated. In [28], Jens Tambke suggests, for example, to use the "Theory of inertially coupled with profiles", which seems to estimate the wind mean profile well for FINO-1. Another possibility is to apply the Computational Fluid Dynamics (CFD). It has been shown in the COSMO-EU model analysis that the results were satisfying, thus a more accurate local model should generate good wind speed estimations. Indeed, the results from the DWD database are encouraging and the COSMO-EU model should be analysed using other offshore locations to check its reliability in wind speed profile estimation.

The offshore wind speed profile is a difficult phenomenon to simulate due to the several aspects explained and the current methodologies do not reach the desired accuracy. Some improvements in wind profile estimation have to be done for offshore wind energy applications. For this reason we have to improve our tools for a realistic assessment of the offshore wind speed profile.

"I can't change the direction of the wind, but I can adjust my sails to always reach my destination."

Jimmy Ray Dean

REFERENCES

[1] R. B. Stull, *An Introduction to Boundary Layer Meteorology*, Kluwer Academic Publishers, 1988.

[2] I. Troen, E. L. Petersen, *European Wind Atlas*, Risø National Laboratory, Roskilde, Denmark, 1989.

[3] N. G. Mortensen, L. Landerberg, I. Troen, E. L. Petersen, Wind Analysis and Application Program (WAsP)-User's Guide. Report Risø-I-666 (EN), Vol. 2, Risø National Laboratory, Roskilde, Denmark, 1993.

[4] T. Foken, 50 Years of the Monin-Obukhov Smilarity Theory, *Boundary-Layer Meteorology*, Vol. 119, N. 3, pp. 431-44, 2006.

[5] A.J.M. Van Wijk, A.C.M. Beljaars, A.A.M. Holtslag and W.C. Turkenburg, Evaluation of Stability Corrections in Wind Speed Profiles Over the North Sea, *Journal of Wind Engineering and Industrial Aerodynamics*, Vol. 33, pp. 551-566, 1990.

[6] A. Sathe, W. Bierbooms, Influence of Different Wind Profiles due to Varying Atmospheric Stability on the Fatigue Life of Wind Turbines, *The Science of Making Torque from Wind*, IOP Publishing, 2007.

[7] B. Lange, S.Larsen, J. Højstrup,R. Barthelmie, The Wind Speed Profile at Offshore Wind Farm Sites, *Proceedings of DEWEK 2002*, 2002.

[8] B. Lange, Modelling The Marine Boundary Layer for Offshore Wind Power Utilisation, PhD Thesis, Universität Oldenburg, 2002.

[9] B. Lange, S.Larsen, J. Højstrup,R. Barthelmie, A Fetch Dependent Model of Sea Surface Roughness for Offshore Wind Power Utilisation, *Proceedings of the European Wind Energy Conference 2001*, pp. 830-833, 2001

[10] B. Lange, S.Larsen, J. Højstrup,R. Barthelmie, Importance of Thermal Effects and Sea Surface Roughness for Offshore Wind Resource Assessment, *Journal of Wind Engineering and Industrial Aerodynamics*, Vol. 92, pp. 959-988, 2004.

[11] B. Lange, S.Larsen, J. Højstrup,R. Barthelmie, Evaluation of Models for the Vertical Extrapolation of Wind Speed Measurements at Offshore Sites. EWEA, Offshore Wind Energy special topic conference, Brussels (BE), 2001.

[12] H. Charnock, Wind Stress Over a Water Surface, *Quar. J. R. Meteorol. Soc.*, Vol. 81, pp. 639-640, 1955.

[13] IEC 61400-3 (Draft). PART 3: Design Requirements for Offshore Wind Turbines, IEC TC88 WG3: Committee Draft, December 2005.

[14] M.Motta, RJ Barthelmie, P Vølund. The Influence of Non-logarithmic Wind Speed Profiles on Potential Power Output at Danish Offshore Sites, *Wind Energy*, Vol. 8, pp. 219-236, 2005.

[15] A. Grachev, C. Fairall, Dependence of the Monin-Obukhov Stability Parameter on the Bulk Richardson Number Over the Ocean, *Journal of Applied Meteorology*, Vol. 36, pp. 406-415, 1996.

[16] C.W. Fairall, E. F. Bradley, J.S. Godfrey, G.A. Wick, J. B. Edson and G.S. Young, Cool-Skin and Warm-Layer Effects on Sea Surface Temperature, *Journal of Geophysical Research*, Vol. 101, pp. 1295–1308, 1996.

[17] R. Berkowicz, L.P. Prahm. Evaluation of the Profile Method for the Estimation of the Surface Fluxes of Momentum and Heat, *Atmospheric Environment*, Vol. 16, 1982.

[18] H. W. Bitzer, J. Steppeler, Documentation of the Z−Coordinate Dynamical Core of LM, Technical Report, N. 6, 2004 (www.cosmo−model.org).

[19] www.dwd.de

[20] www.fino-offshore.com

[21] www.windspeed.co.uk

[22] www.thiesclima.com

[23] H.J. Kouwenhoven, User Manual Data Files Meteorological Mast NoordzeeWind, 2007.

[24] www.mierijmeteo.com

[25] www.vaisala.com

[26] B. Lange, S. Larsen, J. Højstrup, R. Barthelmie, The Influence of Thermal Effects on the Wind Speed Profile of the Coastal Marine Boundary Layer, *Boundary-Layer Meteorology*, Vol. 112, N. 3, pp. 587-617, 2004.

[27] www.noaa.gov

[28] J. Tembke, L. Claveri, J. Bye, C. Poppinga, B. Lange, L. von Bremen, F. Durante, J. Wolff, Offshore Meteorology for Multi-Mega-Watt Turbines, *Proceedings EWEC 2006*, 2006.

[29] M. G. Lawrence, The Relationship Between Relative Humidity and the Dew Point Temperature in Moist Air: A simple Conversion and Applications, *Bull. Am. Meteorol. Soc.*, Vol. 86, pp. 225-233, 2005.

[30] www.gorhamschaffler.com

[31] mtp.jpl.nasa.gov

[32] www.noordzeewind.nl

[33] P.J. Ecen, Meteorological Measurements OWEZ, ECN Report, 2007.

Appendix A

The constants and equations applied for the analyses but not yet explained are reported in this section.

Constants	**FINO-1**	**Egmond aan Zee**
ρ	1.22 kg/m^3	
g	9.81 m/s^2	
P_0	100000 [Pa]	
c_p	1003.5 [J /kg K]	
R_{air}	287 [J/ kg K]	
k	0.4	
R	8.314 [J/mol K]	
M	0.02896 [kg/mol]	
ε_a	0.622	
f_c	$1.46 \cdot e^{-4} \cdot \sin(lat)$	
L_v	2.501e6 [J/kg]	
lat	54°	52.60°
$DALR$	- 9.8 [K/km]	
C	10	
C_1	5	

Table A.1: Constants applied in the models.

Equations:

$$P = P_0 \cdot e^{\frac{-g \cdot M \cdot z}{R \cdot T}} \tag{A.1}$$

A.1 represents the air pressure at elevation *z* for the air temperature *T*.

$$Es = 6.11 \cdot 10^{\frac{7.5 \cdot (T - 273.16)}{237.7 + (T - 273.16)}} \tag{A.2}$$

A.2 shows the equation of the saturation vapor pressure for the air temperature *T* [30].

$$T_v = \frac{T}{1 - \frac{Es \cdot RH}{100 \cdot P} \cdot (1 - \varepsilon_a)} \tag{A.3}$$

A.3 is the virtual air temperature [31].

$$\theta_v = T_v \left(\frac{P_0}{P} \right)^{\frac{R_{air}}{c_p}} \tag{A.4}$$

A.4 is the equation of the virtual potential temperature.

$$\theta = T \left(\frac{P_0}{P} \right)^{\frac{R_{air}}{c_p}} \tag{A.5}$$

And, similarly, A.5 is the potential temperature.

$$RH = 100 - 5 \cdot \left(T - T_D \right) \tag{A.6}$$

A.6 shows the equation relating relative humidity *RH* and dew temperature T_D [29].